Economic Geology

BULLETIN OF THE SOCIETY OF ECONOMIC GEOLOGISTS

VOL. 112 March–April NO. 2

What Caused the Formation of the Giant Bingham Canyon Porphyry Cu-Mo-Au Deposit? Insights from Melt Inclusions and Magmatic Sulfides*

Daohan Zhang[1,2] and Andreas Audétat[2,†]

[1] *Faculty of Earth Resources, China University of Geosciences, Wuhan 430074, China*

[2] *Bayerisches Geoinstitut, University of Bayreuth, 95440 Bayreuth, Germany*

Abstract

Porphyry Cu deposits are commonly thought to have formed by magmas that were unusually rich in metal and/or sulfur. In this study, we test this assumption by reconstructing the metal and sulfur content of an ore-related latite magma at Bingham Canyon and comparing it with that of intermediate magmas in several other arc magma systems. The ore-related latite magma at Bingham Canyon records strong evidence for magma mixing and has a major to trace element composition that can successfully be modeled by a mixture of ~40 wt % mafic magma, which was similar to the most mafic rock found at Bingham Canyon (a melanephelinite containing 45 wt % SiO_2), and ~60 wt % felsic magma of rhyolitic composition. Based on the modal abundance of 0.19 ± 0.01 vol % sulfides and laser ablation-inductively coupled plasma-mass spectrometry analyses of unaltered sulfide inclusions preserved within hornblende and plagioclase phenocrysts, the latite magma contained 50 to 90 ppm Cu, 0.8 to 2.0 ppb Au, 2 to 3 ppm Mo, and ≥0.12 to 0.14 wt % S. Whole-rock and melt and sulfide inclusion data suggest that the bulk of copper and Au in the latite magma was derived from the mafic end member, whereas significant amounts of sulfur were also provided by the felsic end member. A rough, independent estimate of the amount of Cu present in the mixed magma can be obtained by taking the Cu content of mafic, sulfide-undersaturated silicate melt inclusions and multiplying it with the mass fraction of mafic magma involved in the magma mixing.

Applying this latter approach to two other porphyry Cu-mineralized magma systems (Santa Rita, USA; Bajo de la Alumbrera, Argentina) and several modern arc magma systems suggests that ore-forming intermediate magmas in mineralized systems were not unusually Cu rich. Whether or not they were unusually sulfur rich could not be answered with the available data. If the sulfur contents of mineralizing magmas prove to be normal, then the most distinctive feature of fertile magma systems may be the formation of large, long-lived magma chambers at 5- to 15-km depth and the development of vent structures that enable focused fluid flow.

Introduction

The formation of porphyry Cu (-Mo, Au) deposits involves a specific sequence of steps, including (1) dehydration of subducting oceanic lithosphere, (2) ascent of hydrous fluids/melts, (3) partial melting of the mantle wedge, (4) ponding of the partial melts at the crust-mantle boundary, where they undergo magma assimilation, storage, and homogenization (MASH) processes, (5) further magma ascent, (6) formation of upper-crustal magma chambers, (7) exsolution of volatiles, (8) fluid focusing, and (9) precipitation of ore metals (e.g., Richards, 2003, 2005; Sillitoe, 2010). All of these processes also operate to some extent in unmineralized arc magma systems. The key to understanding the formation of porphyry Cu (-Mo, Au) systems is thus to identify those parameters that were different in mineralized magma systems compared to barren magma systems. Many possibilities have been proposed in previous studies, including the size (e.g., Cloos, 2001; Richards, 2005), depth (e.g., Richards, 2005; Sillitoe, 2010), and shape (e.g., Richards, 2005) of the underlying magma chamber, the lifetime of the magma system (e.g., Richards, 2005; Mpodozis and Cornejo, 2012), and the magma water content (e.g., Loucks, 2014). However, perhaps the most popular hypothesis is that mineralizing magmas are enriched in metal and/or sulfur (e.g., Halter et al., 2005; Core et al., 2006; Stern et al., 2007; Richards, 2009; Jenner et al., 2010).

The main aim of the present study is to test this latter hypothesis by reconstructing the metal and sulfur content of the ore-forming magma at Bingham Canyon and comparing it with results from several other porphyry Cu-mineralized and barren arc magma systems. A major difficulty of this approach is to obtain reliable estimates of original sulfur and metal contents of a given magma. Whole-rock analyses are only of limited use because sulfur and chalcophile elements are commonly lost from the magma during or after its solidification. Silicate melt inclusions (here called melt inclusions) are better, but they provide information only on the composition of

† Corresponding author: e-mail, andreas.audetat@uni-bayreuth.de

*A digital supplement to this paper is available at http://economicgeology.org/ and at http://econgeol.geoscienceworld.org/.

, Vol. 112, pp. 221–244
0361-0128/17/4467/221-24

Submitted: January 25, 2016
Accepted: July 21, 2016

the silicate melt rather than that of the bulk magma. In order to estimate the metal and sulfur content of a bulk magma, it is necessary to determine the abundance of all phases (including sulfides and sulfates) present in the magma and to quantitatively constrain the distribution of elements among these phases.

Geologic Background

The giant Bingham Canyon porphyry Cu-Mo-Au deposit is situated in the eastern part of the Oquirrh Mountains, which are located about 30 km southwest of Salt Lake City, Utah. The Oquirrh Mountains consist of Paleozoic sedimentary rocks (mainly arkosic orthoquartzites, limestones, and calcareous siltstones), into which magmas were intruded during Eocene to Oligocene times. Magma ascent and emplacement appear to have been controlled by the E-W–trending Uinta axis, which represents an old structural boundary separating Archean crust in the north from Paleoproterozoic terrane in the south (Stewart et al., 1977; Karlstrom et al., 2005).

Igneous activity in the Oquirrh Mountains started when the regional tectonic setting changed from compression to weak extension during the late Eocene (English and Johnston, 2004). The Bingham Canyon deposit is hosted within a large volcanoplutonic complex that is composed of rocks ranging in composition from basanite to rhyolite, with latite and monzonite being the dominant lithologies (e.g., Moore, 1973; Waite et al., 1997). The rocks have traditionally been divided into an older volcanic suite, a mafic alkaline suite, an intrusive suite, and a younger volcanic suite (Waite et al., 1997; Maughan et al., 2002). The older volcanic suite, the mafic alkaline suite, and the intrusive rocks are all roughly coeval with K-Ar ages ranging from 38.6 to 37.8 Ma (Parry et al., 2001). The intrusive sequence starts with passive emplacement of a large, equigranular mass of monzonite (~58 wt % SiO_2, forming the Bingham stock and Last Chance stock) into the base of the developing stratovolcano. The Bingham stock is intruded by a mass of quartz monzonite porphyry (~62 wt % SiO_2) that is associated with the main pulse of Cu-Au mineralization. Both the Bingham stock and the quartz monzonite porphyry are cut by a series of NE-trending porphyry dikes of latitic to quartz latitic composition (57–64 wt % SiO_2; Moore, 1973) that are also mineralized, but to a lesser extent than the quartz monzonite porphyry. The latite dikes record evidence for substantial mixing with more mafic magma. U-Pb zircon age data by von Quadt et al. (2011) suggest that all porphyritic intrusives were emplaced between 38.1 and 37.8 Ma. A narrow minette dike (57.9 wt % SiO_2) that cuts through the quartz monzonite porphyry in the Bingham deposit has been dated at 37.7 ± 0.1 Ma by Deino and Keith (1997). This age is indistinguishable from that of melanephelinite lava flows (37.8 ± 0.1 Ma) in the upper part of the older volcanic sequence. Deep-seated Mo mineralization overprints the youngest quartz latite porphyry dike and was dated at 37.3 to 36.8 Ma by molybdenite Re-Os (Chesley and Ruiz, 1997; Seo et al., 2012). Subsequent intrusives located several km southeast of the mine area include the volcanic plugs of the Step Mountain Andesite (36.3 ± 0.2 Ma) and the Shaggy Peak Rhyolite (35.5 ± 0.1 Ma). In summary, crosscutting relationships, age data, and geochemical evidence suggest that the Bingham Canyon magma system follows a broad evolution from monzonitic/latitic composition toward rhyolitic composition, interrupted by incursion of mafic alkaline magma and related magma mixing after the emplacement of the quartz monzonite porphyry. Because both the quartz monzonite porphyry and the mixed latite porphyry dikes are mineralized, it has been proposed that mafic alkaline magma was already present at the base of the magma chamber during the main mineralization event and that this mafic alkaline magma played a key role in providing sulfur and metals (Keith et al., 1997; Waite et al., 1997).

Methods

To reconstruct the evolution of sulfur and metals in the Bingham magma system, samples from different rock types ranging from the most mafic magma (melanephelinite; 45 wt % SiO_2) to the most felsic (rhyolite; 74 wt % SiO_2) were investigated (Table 1). Sample locations are shown in Figure 1b, and relevant information is summarized in Table 1. In this study, we mainly focused on melt and sulfide inclusions because the former retain original concentrations of metals and volatiles, and the latter are a major host of ore-forming metals (e.g., Cu and Au) in the magma. From each sample, one or two polished sections of 100- to 300-μm thickness were prepared and subsequently examined in a standard petrographic microscope. Small mineral inclusions within phenocrysts that could not be identified optically were identified using a Horiba Scientific LabRAM HR800 Raman spectrometer equipped with a 632.8-nm HeNe laser source.

Melt inclusions, sulfide inclusions, minerals, and fine-grained rock matrices were analyzed by laser ablation-inductively coupled plasma-mass spectrometry (LA-ICP-MS). The utilized system consists of a 193-nm ArF Excimer laser (GeolasPro system, Coherent, USA) attached to a quadrupole mass spectrometer (Elan DRC-e, Perkin Elmer, Canada). Analyzed isotopes include ^{11}B, ^{23}Na, ^{25}Mg, ^{27}Al, ^{28}Si, ^{31}P, ^{32}S, ^{39}K, ^{43}Ca, ^{49}Ti, ^{51}V, ^{53}Cr, ^{55}Mn, ^{57}Fe, ^{59}Co, ^{60}Ni, ^{65}Cu, ^{66}Zn, ^{75}As, ^{82}Se, ^{85}Rb, ^{88}Sr, ^{89}Y, ^{90}Zr, ^{93}Nb, ^{98}Mo, ^{105}Pd, ^{107}Ag, ^{111}Cd, ^{121}Sb, ^{125}Te, ^{133}Cs, ^{137}Ba, ^{139}La, ^{140}Ce, ^{181}Ta, ^{195}Pt, ^{197}Au, ^{205}Tl, ^{208}Pb, ^{209}Bi, ^{232}Th, and ^{238}U. The laser was operated at 5 to 10 Hz and an energy density of 3 to 10 J/cm^2 on the sample surface, using laser pits ranging from 15 to 80 μm in diameter. The fine-grained rock matrices were analyzed with an 80-μm pit and the sample was moved during ablation, resulting in a total ablation area of ~1,000 μm^2. Three densely pressed powder pellets prepared from finely ground ($\leq$10 μm grain size) bulk samples were analyzed in a similar fashion in order to obtain "bulk-rock" analyses.

The sample chamber was flushed with He gas at a rate of 0.4 l/min, and 5 ml/min H_2 gas was added on the way to the ICP-MS (Guillong and Heinrich, 2007). Analyzed isotopes were measured using dwell times of 10 to 50 ms per isotope. The ICP-MS system was tuned to a ThO rate of 0.07 ± 0.02% and a rate of doubly charged Ca ions of 0.20 ± 0.02% based on measurements on NIST SRM 610 glass.

Entire, unexposed melt inclusions (both crystalline and glassy) were drilled out of the surrounding host mineral, and excess ablated host was subtracted numerically from the resulting LA-ICP-MS signals to obtain the melt composition (Halter et al., 2004a; Pettke, 2006). External standardization was based on NIST SRM 610 glass (Jochum et al., 2011).

Table 1. Mineralogy, Inclusion Types, and Relation to Mineralization of Investigated Rocks from the Bingham Canyon Magma System

Rock type	Melanephelinite	Shoshonite	Pyroxene-latite	Latite	Andesite	Rhyolite
Age (Ma)[1]	37.82 ± 0.14	~37.8	?	38.84 ± 0.19	36.26 ± 0.18	35.49 ± 0.13
Sample no.	Bing 1, Bing 2, Bing 3	Bing 4	Bing 19	Bing 12, Bing 13, Bing 14	Bing 6	Bing 8
Whole-rock SiO_2 (wt %)	~44.5	53.6–58.6	57.6–60.4	58.2–64.5	57.5–62.5	67.9–74.0
Phenocrysts (vol %)	Ol (20–25; fo_{85-90}), phl (~3), cpx (1–3)	Cpx (10–15), bio (7–10), ol (3–5; fo_{88-89})	Plag (20–25; an_{37-47}), cpx (15–20), bio (5–7), mgt (<1)	Hbl (20–30), plag (5–10; an_{40-50}), bio (5–10), ol† (5–10), mgt (~1), cpx (≤1)	Plag (15–20; an_{29-32}), bio (7–10), hbl (7–10), cpx (~5), qtz (3–5)	Qtz (25–30), plag (10–15), bio (~5)
Mineral inclusions in phenocrysts	Phl, spl	Mgt, sulf	Mgt, apa, sulf	Mgt, ilm, zirc, apa, chr, hem, sulf, anhy	Mgt, ilm, sulf, anhy	
Host of analyzed MIs	Ol	Ol	Plag	Plag	Qtz, plag	Qtz
Relation to mineralization	Syn mineralization (?)	Syn mineralization (?)	Syn mineralization (?)	Syn mineralization	Post mineralization	Post mineralization

Abbreviations: an = anorthite component, anhy = anhydrite, apa = apatite, bio = biotite, chr = chromite, cpx = clinopyroxene, fo = forsterite component, hbl = hornblende, hem = hematite, ilm = ilmenite, mgt = magnetite, MIs = melt inclusions, ol = olivine, ol† = altered olivine, phl = phlogopite, plag = plagioclase, qtz = quartz, spl = spinel, sulf = sulfide, zirc = zircon

[1] Age data are from Deino and Keith (1997) and Biek et al. (2005)

Internal standardization of melt inclusions hosted in olivine and plagioclase was based on SiO_2 vs. MgO trends displayed by whole-rock data (Waite et al., 1997; Maughan et al., 2002; Biek, 2006; Stavast et al., 2006), whereas for quartz-hosted melt inclusions SiO_2 vs. Al_2O_3 whole-rock trends were used. In all cases, the sum of major element oxides was normalized to 100 wt %. Sulfide inclusions were quantified using a synthetic pyrrhotite (Po724 T3 SRM of the Memorial University of Newfoundland) as external standard for Fe and S, and NIST SRM 610 for all other elements, and then normalizing the sum of S, Fe, Ni, and Cu to 100 wt %. This approach was also used to measure the sulfide standard MSS5 described in Brenan (2015), which was thoroughly characterized by electron microprobe, solution-ICP-MS, and LA-ICP-MS and contains 57.93 ± 0.2 wt % Fe, 39.76 ± 0.14 wt % S, 1.07 ± 0.01 wt % Ni, 223 ± 17 ppm Cu, 80 ± 7 ppm Se, 59 ± 3 ppm Sb, 43 ± 3 ppm Te, and 71 ± 1 ppm Pb. Additionally, the approach was used to measure chalcopyrite, bornite, and chalcocite as unknowns. In all cases, the results agree within 7% with the reference/theoretical values (supplementary Table S1), for which reason we regard the approach using two separate external standards as valid. For altered sulfides, we used the average Fe content of fresh sulfides as an internal standard because Fe appears to have behaved conservatively during sulfide alteration (see below). Analyses of Fe-Ti oxides were quantified based on ilmenite KI-2193 collected by Tony Morse (major elements; composition given in Janssen et al., 2010) and NIST SRM 610 (minor to trace elements) as external standards and then normalizing the sum of all major element oxides to 100 wt %. Silicate minerals and analyses of fine-grained rock matrices were quantified using NIST SRM 610 glass as an external standard and then normalizing the sum of all major element oxides to 100 wt %. Uncertainties associated with the analyses of sulfides, oxides, silicate minerals, rock matrices, and quartz-hosted melt inclusions are believed to be ≤5 to 7%, except for elements close to the detection limit. For melt inclusions hosted in olivine and plagioclase, the uncertainties are distinctly higher (10–20% for all elements) due to difficulties constraining the internal standard (see below).

Unexposed melt inclusions within olivine phenocrysts from the melanephelinite of Bingham Canyon (sample Bing1 to Bing3) were rehomogenized for 48 hours at 1,100°C and 1.5-kbar confining Ar pressure in rapid-quench TZM cold-seal pressure vessels. Clinopyroxene-hosted melt inclusions from the two most mafic magmas identified at Santa Rita, New Mexico, were rehomogenized in a similar manner at 1,050°C. After exposing selected rehomogenized melt inclusions on the surface by polishing, they were analyzed by electron microprobe for major elements plus S, Cl, and F. These analyses were performed on a JEOL JXA-8200 microprobe equipped with five spectrometers and TAP, PET, LiF, and LDE1 spectrometer crystals, using 15 kV, 20 nA, and a beam defocused to 3 to 10 μm. Na and K were measured for 10 s on peak and 5 s on each background (10/2 × 5), Si, Al, Ti, Fe, Mn, Mg, and Ca with 20/2 × 10, and F, Cl, and S with 60/2 × 30. Na, K, Si, S, and Fe were measured first. Time-resolved signals showed up to 10% loss of Na in the most hydrous glasses, but no loss of Cl and F. Standardization was performed on albite (Na, Si), orthoclase (K), spinel (Al), $MnTiO_3$ (Mn, Ti), metallic Fe, enstatite (Mg), wollastonite (Ca), fluorite (F), vanadinite

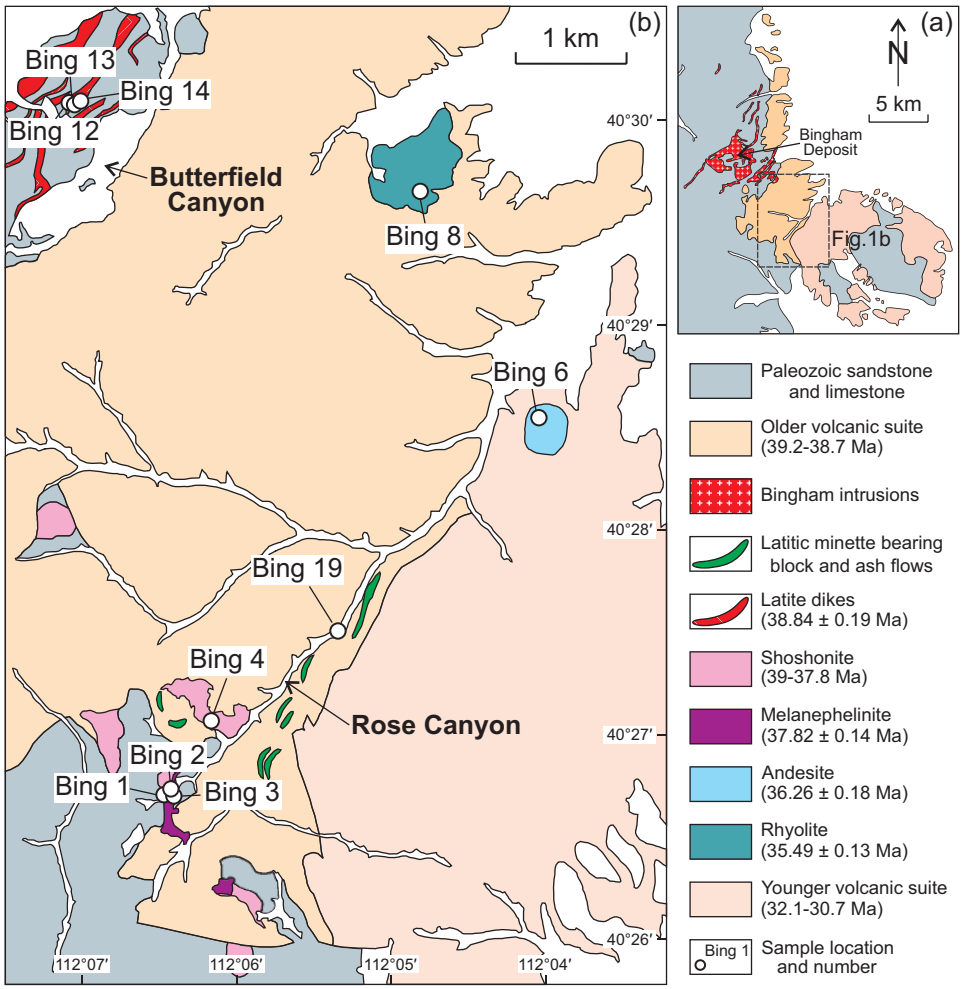

Fig. 1. (a) Simplified geologic map of the eastern Oquirrh Mountains, showing the location of the Bingham deposit and the study area (modified after Waite et al., 1997). (b) Geologic map of the study area (Butterfield Canyon and Rose Canyon), showing the locations of samples that were investigated in this study (modified after Maughan et al., 2002; Biek et al., 2005, 2007).

(Cl), and barite (S). A topaz crystal containing 20.5 ± 0.5 wt % F, according to XRD measurements and equations for cell parameters given in Alberico et al. (2003), was measured as unknown and returned correct F values of 20.2 ± 0.3 wt % F.

Results

Sample petrography

Fresh samples of melanephelinite (samples Bing1, Bing2, and Bing3) are dark green in color and contain phenocrysts of olivine (20–25 vol %; $Fo_{85–90}$) and phlogopite (~3 vol %), and a few of clinopyroxene (1–3 vol %; Fig. 2a). Published whole-rock analyses of this rock type contain 44 to 46 wt % SiO_2 and plot in the basanite field of the total alkali vs. silica (TAS) diagram (Maughan et al., 2002). The olivine phenocrysts measure up to 3 mm in length and are mostly unzoned. They contain abundant Cr spinel inclusions and rare inclusions of phlogopite and crystallized melt inclusions (Fig. 3a). A few olivine phenocrysts contain Cr- and Ni-rich cores that are characterized by particularly abundant Cr spinel inclusions. Clinopyroxene phenocrysts have a greenish color, are much smaller (<0.5 mm), and commonly exhibit distinctive core-rim textures (Fig. 2e) with dark green, Fe-, V-, and Zr-rich cores and light green, Mg-, Cr-, and Ni-rich rims. Only a few very small melt inclusions are present in the clinopyroxene phenocrysts. Despite careful screening, no sulfide inclusions were found in olivine and clinopyroxene phenocrysts. This evidence suggests that the melanephelinite magma was sulfide undersaturated, as was also concluded in previous studies (Waite et al., 1997; Maughan et al., 2002). However, barite inclusions were not found either, which contrasts with the finding of Maughan et al. (2002).

A sample of shoshonite (Bing4; 55 wt % SiO_2) is greenish gray in color and contains phenocrysts of clinopyroxene (10–15 vol %), biotite (7–10 vol %), and olivine (3–5 vol %; $Fo_{88–89}$) in an aphanitic groundmass (Fig. 2b). Many of the clinopyroxene phenocrysts show obvious core-rim textures (Fig. 2f) with dark green, often sieve textured cores, and light green rims. As in the case of the melanephelinite, the cores are rich in Fe, V, and Zr, whereas the rims are rich in Mg, Cr, Ni, and Sr—i.e., the grains are reversely zoned. Melt inclusions are very rare in this rock; only one single inclusion hosted in olivine could be

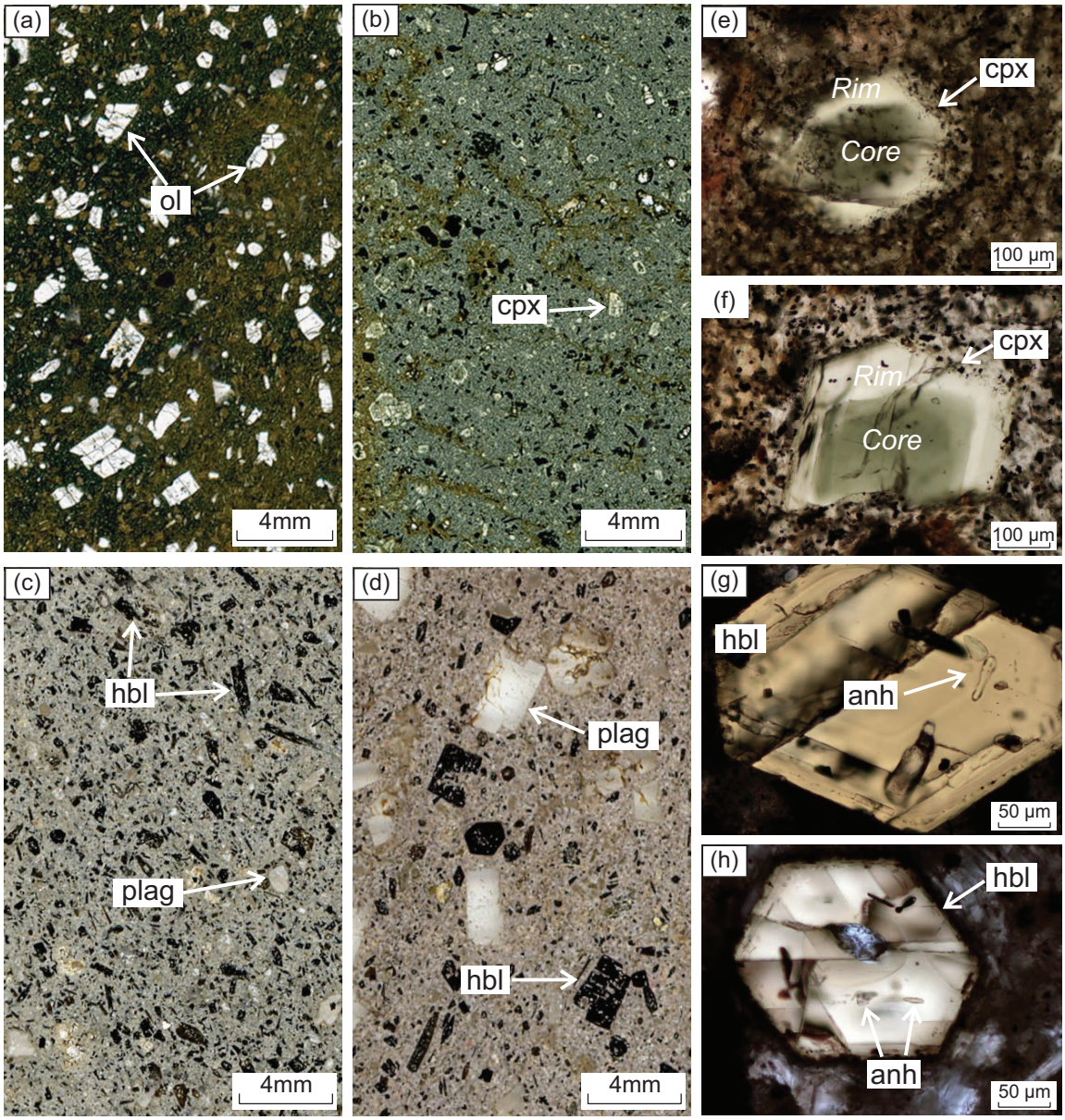

Fig. 2. Photographs of polished thick sections and individual phenocrysts from different rock types. Polished thick sections are from melanephelinite (a), shoshonite (b), latite (c), and andesite (d). Clinopyroxene phenocrysts from melanephelinite (e) and shoshonite (f) show core-rim textures with dark green cores and light green rims. Anhydrite inclusions are common in hornblende phenocrysts from latite (g) and andesite (h). Images (a) through (d) were taken with incident light, while images (e) through (h) were taken in transmitted light. Abbreviations: anh = anhydrite, cpx = clinopyroxene, hbl = hornblende, ol = olivine, plag = plagioclase.

analyzed. On the other hand, magmatic sulfide inclusions are abundant and are hosted mainly in clinopyroxene (Fig. 4a).

A hand specimen of a pyroxene-bearing latite (Bing19; 60 wt % SiO_2; collected from a large boulder on the valley floor of Rose Canyon) is dark gray in color and contains phenocrysts of plagioclase (20–25 vol %; $An_{37–47}$), clinopyroxene (15–20 vol %), biotite (5–7 vol %), and minor magnetite (<1 vol %) in an aphanitic groundmass. The plagioclase phenocrysts contain abundant crystallized melt inclusions (Fig. 3b) and apatite inclusions plus some magnetite inclusions, whereas the clinopyroxene phenocrysts host fewer melt inclusions that are either glassy or crystallized. Magmatic sulfide inclusions are rare, but present, in this rock. Several small sulfide inclusions (<10 μm in diameter) were found in clinopyroxene.

Samples of latite (Bing12, Bing13, and Bing14; 58–61 wt % SiO_2) were taken from the same sill in Castro Gulch that has been studied in detail by Stavast et al. (2006). They contain phenocrysts of hornblende (20–30 vol %), plagioclase (5–10 vol %; $An_{40–50}$), biotite (5–10 vol %), quartz (~1 vol %), and magnetite (~1 vol %) set in a dark gray, fine-grained matrix (Fig. 2c). Altered remains of a mafic phenocryst phase (5–10 vol %; most likely olivine) are present, as well. A single clinopyroxene phenocryst/xenocryst was observed in sample

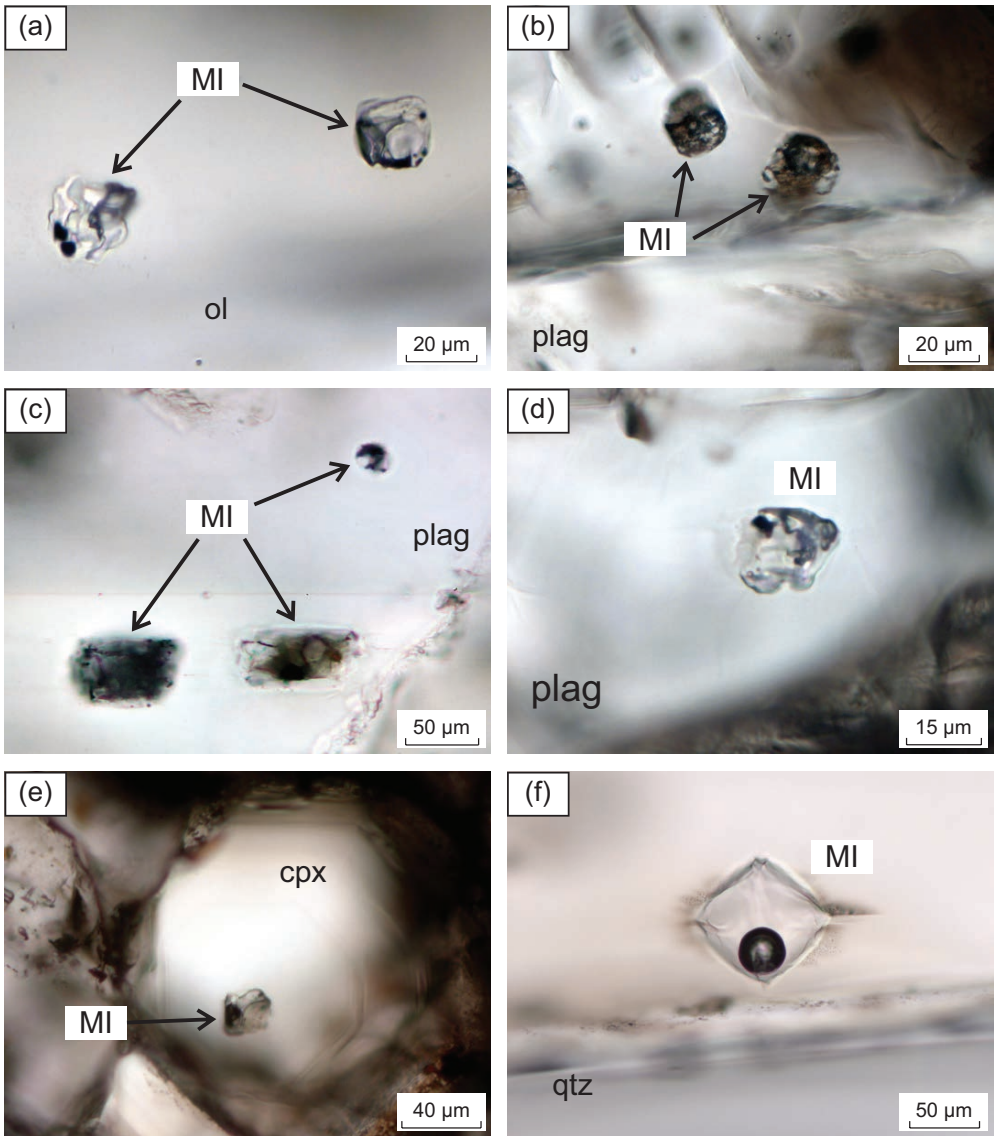

Fig. 3. Examples of melt inclusions (MI) within various host minerals. (a) Crystallized melt inclusions in olivine (ol) from melanephelinite. (b) Crystallized melt inclusions in plagioclase (plag) from pyroxene-latite. (c) Crystallized melt inclusions in plagioclase from latite. (d) Crystallized melt inclusions in plagioclase from the Step Mountain Andesite. (e) Crystallized melt inclusions in clinopyroxene (cpx) from the Step Mountain Andesite. (f) Glassy melt inclusions in quartz (qtz) from the Shaggy Peak Rhyolite. Abbreviations: cpx = clinopyroxene, ol = olivine, plag = plagioclase, qtz = quartz.

Bing14. Abundant magmatic sulfide inclusions are present in the hornblende phenocrysts of all latite samples. They are fresh if completely surrounded by hornblende (Fig. 4b) but partially to completely altered to a fine-grained aggregate of magnetite ± pyrite if intersected by cracks (Fig. 4c). Similar aggregates of fine-grained magnetite ± pyrite occurring in the rock matrix (Fig. 4d) represent decomposed sulfide blebs (Larocque et al., 2000; Stavast et al., 2006). Another common type of magmatic inclusion in hornblende phenocrysts is anhydrite (Fig. 2g). Plagioclase phenocrysts host solid inclusions of spinel, magnetite, ilmenite, and rare anhydrite. Magnetite phenocrysts usually contain 10.7 to 13.3 mol % ulvöspinel; however, in sample Bing14, an additional magnetite population occurs that contains 20.6 to 21.0 mol % ulvöspinel and is intergrown with ilmenite containing a 57.1 to 57.5 mol % $FeTiO_3$ component. A single microphenocryst of zircon was observed, as well. Melt inclusions are abundant in plagioclase, where they are either crystallized or glassy (Fig. 3c), but they are rare in hornblende, where they are mostly glassy.

The andesite from Step Mountain (Bing6 in Fig. 1b) is light gray in color and contains phenocrysts of plagioclase (15–20 vol %; $An_{29–32}$), biotite (7–10 vol %), hornblende (7–10 vol %), clinopyroxene (~5 vol %), quartz (3–5 vol %), and <1 vol % of magnetite and ilmenite set in a fine-grained groundmass (Fig. 2d). Rare titanite phenocrysts (with ilmenite reaction rims) are present, as well. Several hornblende grains display core-rim textures with dark cores and bright rims. Magnetite is present both as small phenocrysts in matrix and as inclusions within hornblende and contains 16.5 to 20.0 mol % ulvöspinel. A few magnetite inclusions coexist

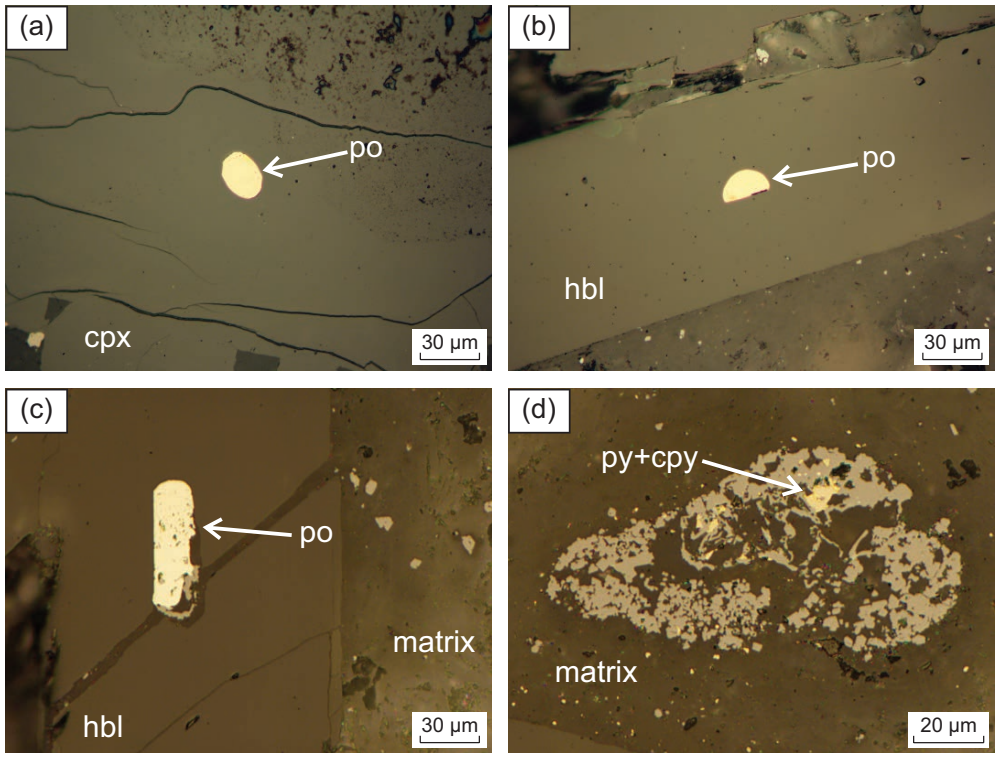

Fig. 4. Reflected-light photomicrographs of sulfide inclusions. (a) Sulfide inclusions in clinopyroxene (cpx) from shoshonite. (b, c) Sulfide inclusions in hornblende from latite. The sulfide inclusion in (c) was intersected by a crack and thus is partly altered to iron oxides at its lower end. (d) Large sulfide inclusion in the matrix of the latite. The sulfide inclusion is almost completely altered to iron oxides (gray minerals), which occupy ca. 50% of the original sulfide inclusion volume. Abbreviations: cpx = clinopyroxene, cpy = chalcopyrite, hbl = hornblende, po = pyrrhotite, py = pyrite.

with inclusions of ilmenite in the same hornblende phenocrysts, allowing reconstruction of temperature and f_{O_2}. Moreover, inclusions of anhydrite are present in the hornblende (Fig. 2h). Melt inclusions (commonly crystallized) are abundant in plagioclase (Fig. 3d) and quartz but rare in clinopyroxene (Fig. 3e), while sulfide inclusions are present dominantly in hornblende (Fig. 2h).

The rhyolite from Shaggy Peak is light gray in color and contains phenocrysts of plagioclase, quartz, and biotite. Many large, glassy melt inclusions are preserved within the quartz phenocrysts (Fig. 3f). No sulfide inclusions were observed in this rock.

Thermobarometry

To estimate the preemplacement crystallization conditions of the magmas, the following methods were applied: (1) Al-in-olivine thermometry of spinel-bearing magmas (Coogan et al., 2014); (2) Ti-in-phlogopite thermometry (Righter and Carmichael, 1996); (3) zircon saturation thermometry (Watson and Harrison, 1983); (4) Fe-Ti oxide thermometry and oxybarometry (Lepage, 2003, using the normalization scheme of Stormer, 1983, and the calibration of Andersen and Lindsley, 1985); and (5) amphibole-plagioclase thermometry (Holland and Blundy, 1994). The results are summarized in Table 2, whereas the corresponding compositional data are provided in supplementary Tables S2 and S6.

In the melanephelinite, both spinel and phlogopite are present as well-preserved inclusions within olivine phenocrysts, suggesting these three minerals were in equilibrium with each other. Al-in-olivine thermometry yields crystallization temperatures of 1,140° to 1,160°C, consistent with temperature estimates of 1,130° to 1,140°C based on Ti-in-phlogopite thermometry performed on unaltered phlogopite inclusions within olivine.

Table 2. Summary of Thermobarometry Results

Magma type	Method	n[1]	T (°C)	log f_{O_2}
Melanephelinite	Al-in-olivine	5	1,140–1,160	
	Ti-in-phlogopite	5	1,130–1,140	
Shoshonite	Apatite saturation	1	>960	
Pyroxene-latite	Zircon saturation	4	770–840	
	Apatite saturation	4	830–930	
Latite	Zircon saturation	11	760–830	
	Magnetite-ilmenite	4/3	920–960	QFM + (2.2–3.0)
	Plagioclase-hornblende	3/3	750–800	
Andesite	Zircon saturation	7	710–750	
	Magnetite-ilmenite	2/2	870–920	QFM + (2.3–2.6)
Rhyolite	Zircon saturation	4	690–710	

QFM = quartz-fayalite-magnetite
[1] Number of the analyzed grains

For the shoshonite, a minimum temperature was constrained via apatite saturation thermometry based on the SiO_2 and P_2O_5 content of the fine-grained rock matrix. However, the rock does not contain any apatite, implying that the obtained temperature of 960°C represents only a minimum value.

The pyroxene-bearing latite, in contrast, was apatite saturated. Plagioclase-hosted melt inclusions yield apatite saturation temperatures of 830° to 890°C, whereas the less evolved rock matrix yields 930°C. The higher temperature and less evolved composition of the rock matrix compared to melt inclusions (supplementary Table S2) suggest that this magma underwent an event of magma mixing prior to its emplacement.

For the latite samples from Castro Gulch, reconstruction of crystallization conditions is very challenging because these rocks record strong evidence for magma mixing, including (1) coexistence of quartz and olivine (the latter now altered), and (2) the presence of melt inclusions that are distinctly more evolved than the fine-grained rock matrix (see below). However, hornblende phenocrysts commonly contain inclusions of plagioclase, and vice versa, suggesting that these two minerals crystallized partly at the same time. Amphibole-plagioclase thermometry on such coexisting mineral pairs yields temperatures of 750° to 800°C, with values generally decreasing from core to rim. Zircon saturation temperatures calculated from the Zr content of melt inclusions hosted in plagioclase range from 760° to 830°C; magnetite and ilmenite microphenocrysts occurring in the rock matrix return 920° to 960°C; and oxygen fugacities of $\log f_{O_2}$ = QFM + (2.2 – 3.0). These data suggest that the latite of Castro Gulch formed as a result of mixing between a felsic magma with a temperature of ~750°C and a more mafic magma with a temperature of at least 920°C (likely much higher, as the oxides in the matrix probably reflect the temperature after mixing). That efficient mixing between such contrasting magmas is physically possible has been demonstrated, e.g., at Mt. Pinatubo, where mixing between a dacitic magma of ~780°C and a basaltic magma of ~1,200°C produced a hybrid andesite (Pallister et al., 1996).

A similar picture emerges for the Step Mountain Andesite: whereas melt inclusions in plagioclase and quartz are rhyolitic in composition (see below) and yield zircon saturation temperatures of 710° to 750°C, the fine-grained rock matrix is dacitic in composition and yields magnetite-ilmenite temperatures of 870° to 920°C and an oxygen fugacity of $\log f_{O_2}$ = QFM + (2.3–2.6). Therefore, this rock also records mixing between felsic and mafic components shortly before magma emplacement.

Composition of melt inclusions

Although melt inclusions have clear advantages over whole-rock analyses with regard to obtaining information on the abundances of volatiles and metals in magmas, there can be major difficulties in their quantification, especially if they are crystallized. Postentrapment modifications such as partial decrepitation, stretching, diffusive equilibration with the surrounding host mineral, and diffusive loss (or gain) of water are very common phenomena, and most of them cannot be reversed during rehomogenization. Therefore, in the case of crystallized melt inclusions, the reconstruction of original melt compositions is challenging independent of whether they are reheated and then quenched to a glass or analyzed directly by LA-ICP-MS without prior reheating. In either case, it is necessary to use an internal standard to determine the amount of surrounding host that needs to be subtracted from (or, in the case of incomplete rehomogenization, added to) the analysis to obtain the true melt composition (e.g., Halter et al., 2004a; Pettke, 2006; Zajacz and Halter, 2007). For melt inclusions hosted by olivine, diffusive reequilibration between crystallizing melt inclusions and the surrounding host has been shown to result in strong depletions of Fe and Mg in the residual melt, of which only Mg can be reversed during rehomogenization (Danyushevsky et al., 2000). In this study, most melt inclusions were analyzed without prior rehomogenization by LA-ICP-MS, using pit sizes that were significantly larger than the optically visible part of the inclusions, such that material precipitated during sidewall crystallization was included in the signal. Original melt compositions were then calculated by subtracting olivine host until the results fit on the MgO vs. SiO_2 trend defined by whole-rock compositions. There is considerable uncertainty (10–20%) in this approach because of the diffusive equilibration of the trapped melts with their host, and because whole-rock compositions may not follow liquid lines of descent if their formation involved significant amounts of magma mixing, entrainment of cumulate fractions, or subsolidus alteration. However, in the absence of better constraints on the internal standard, it seems to be the best approach available. The results are listed in Table 3 and supplementary Table S2, and are plotted together with whole-rock analyses and rock matrices in Figure 5.

The results obtained for olivine-hosted melt inclusions from the melanephelinite agree well with whole-rock data in terms of FeO, Al_2O_3, CaO, MnO, TiO_2, Nb, Rb, Sr, Y, Zr, Ba, La, and Ce (Fig. 5), whereas the concentrations of Na_2O, K_2O, and P_2O_5 are distinctly higher in the melt inclusions (5.7 ± 0.5 wt %, 5.0 ± 0.6 wt %, and 0.85 ± 0.14 wt %, respectively) than in reported whole-rock analyses (3.6 ± 0.3 wt %, 3.0 ± 0.2 wt %, and 0.41 ± 0.09 wt %, respectively; Table 3; supplementary Table S2). The reason for the mismatch of the latter elements is not clear. In the case of Na and K, it may be due to loss of alkalies from the melanephelinite magma via a volatile phase (as suggested by Elkins-Tanton et al., 2007, for a similar case in Siberian flood basalts), whereas P may be too high in the melt inclusions due to accumulation of this slowly diffusing element in boundary layers around fast-growing phenocrysts (e.g., Kent, 2008). On the other hand, LA-ICP-MS analyses of the fine-grained matrix of the melanephelinite returned P contents similar to those in the melt inclusions (Fig. 5; supplementary Table S2). The Cu content of the melt inclusions is relatively high, ranging from 150 to 280 ppm (average 170 ppm). Four LA-ICP-MS analyses of the fine-grained rock matrix of the melanephelinite returned a slightly more evolved melt composition, with 48 wt % SiO_2, 9 to 11 wt % MgO, and 9 to 11 wt % FeO. The copper content of the rock matrix is highly variable (20–1,400 ppm), substantiating the need of melt inclusions to reconstruct original metal concentrations.

From the shoshonite sample, only a single olivine-hosted melt inclusion could be analyzed. Although the result is again associated with an uncertainty of ~10 to 20%, a composition

Table 3. Representative Compositions of Melt Inclusions and Rock Matrices Analyzed by LA-ICP-MS, Plus Literature Whole-Rock Data

	Major elements (wt %)										Trace elements (ppm)												
Sample name	SiO_2	TiO_2	Al_2O_3	FeO_{tot}	MgO	MnO	CaO	Na_2O	K_2O	P_2O_5	V	Cr	Ni	Cu	Rb	Sr	Y	Zr	Ba	La	Ce	Th	U
Melanephelinite																							
Bing1 MIoliv3 27 μm	43	1.07	11	8.2	16	0.13	8.1	6.5	5.8	1.06	230	200	530	62	160	1,300	28	190	2,900	80	150	10	2
Bing2 MIoliv5 23 μm	40	1.01	12	5.3	17	0.14	12.5	6.1	6	1.01	170	500	790	280	170	1,500	30	170	3,200	78	140	13	1
Bing3 MIoliv13 35 μm	39	0.75	11	9.1	16	0.13	11.8	5.7	5.6	0.78	150	540	2,180	150	160	1,300	23	150	2,700	65	130	9	2
Bing1 matrix2	48	1.11	11	10.6	10	0.18	13.5	3.4	2.7	0.87	220	580	110	1,440	75	1,200	31	230	2,800	85	160	15	2
Bing2 matrix1	48	1.09	10	8.7	11	0.18	15.3	3.2	2.8	0.67	170	780	87	21	87	880	28	240	1,900	70	140	15	3
Avg whole-rock	45	0.96	10	10	16	0.19	10.2	4.1	2.9	0.38	200	960	350	126	79	1,100	23	140	2,100	69	110	8	4
Shoshonite																							
Bing4 matrix1	55	0.91	16	8.6	6.1	0.13	4.7	4.3	4.5	0.72	160	44	77	91	130	990	28	370	2,600	100	180	28	6
Bing4 matrix2	54	0.95	16	9.5	6.5	0.14	4.6	4.3	4	0.72	170	37	83	67	130	970	27	330	2,600	100	190	30	7
Avg whole-rock	56	0.79	13	6.8	7.9	0.12	8	2.8	3.7	0.41	150	600	220	55	99	730	21	190	1,900	78	110	13	3
Pyroxene-latite																							
Bing19 MIplag1 22 μm	69	0.26	17	1.7	0.4	0.03	2.2	5.2	3.9	0.1	25	<11	3	1,550	130	920	14	300	1,900	65	110	26	5
Bing19 MI1plag2 18 μm	71	0.19	17	1.2	0.3	0.02	1.6	6.6	2.9	0.05	17	<14	<3	960	83	550	10	190	1,100	45	64	16	4
Bing19 MI2plag2 21 μm	72	0.16	15	1.2	0.2	0.02	2.4	5.6	3.1	0.05	14	<12	2	400	76	170	8	170	1,000	40	62	15	3
Bing19 matrix1	68	0.49	17	1.9	1.2	0.05	2.9	4	4.8	0.19	50	5	15	19	160	1,200	20	400	2,800	140	250	40	8
Avg whole-rock	59	0.89	14	7.3	5.8	0.07	4.3	2.2	5.7	0.69	130	200	200	1,090	220	750	20	290	2,700	110	180	30	8
Andesite																							
Bing6 MI2plag1 28 μm	74	0.11	15	0.6	0.1	0.02	1	4.5	4.9	0.03	5	<15	<2	83	150	620	7	78	2,400	30	51	16	5
Bing6 MI1plag3 35 μm	73	0.09	14	0.5	0.1	0.02	0.9	3.3	7.9	<0.02	5	<11	<2	130	180	500	9	80	2,100	34	60	16	7
Bing6 matrix2	66	0.67	15	4.5	1.9	0.09	4	3.7	4.3	0.3	79	5	14	53	120	1,400	23	230	3,700	170	300	39	9
Avg whole-rock	60	0.82	16	5.3	3	0.08	5.5	3	2.9	0.35	130	210	44	31	85	870	21	210	1,900	79	140	19	4
Latite																							
Bing12 MI1plag1 30 μm	72	0.17	16	1.3	0.3	0.04	1.9	4.6	3.8	0.06	16	<16	<4	8	110	880	7	190	1,800	62	95	22	5
Bing13 MI3plag2 40 μm	72	0.15	15	1.3	0.3	0.04	2.3	4.1	4.8	0.04	12	<7	2	10	140	660	8	180	2,000	77	110	29	6
Bing14 MI1plag3 40 μm	71	0.22	16	1.6	0.4	0.05	2.1	4.2	4.1	0.05	17	4	1	16	130	840	10	250	1,900	76	130	29	6
Bing12 matrix2	68	0.29	16	3.2	1.7	0.03	2.4	4	4.7	0.2	62	7	28	56	150	830	13	310	2,500	110	170	41	9
Bing13 matrix1	68	0.3	16	2.7	1.7	0.04	2.2	4.1	5	0.09	39	13	34	52	160	710	15	350	2,300	93	140	43	9
Avg whole-rock	61	0.7	15	5	3.3	0.08	4.8	3.1	3.9	0.33	120	130	39	31	120	880	21	270	2,500	84	150	24	5
Rhyolite																							
Bing8 exp.MI1qtz4 50 μm	74	0.06	15	0.43	0.04	0.12	0.5	3.4	6	0.01	<0.3	<4	<1	7	400	4	41	53	6	12	30	20	22
Bing8 MI1qtz3 75 μm	75	0.06	15	0.44	0.04	0.12	0.5	3.9	4.8	0.01	0.2	<3	<1	10	350	3	41	54	4	13	33	23	20
Bing8 MI2qtz3 75 μm	75	n.a.	15	0.43	0.04	n.a.	n.a.	n.a.	n.a.	n.a.	n.a.	n.a.	<3	13	340	3	n.a.	n.a.	4	n.a.	n.a.	n.a.	n.a.
Avg whole-rock	71	0.15	14	1.03	0.2	0.05	0.9	2.4	4.1	0.08	10	69	7	3	130	220	18	91	1,600	31	60	17	5

Notes: Whole-rock data are from Maughan et al. (2002), Waite et al. (1997), Biek (2006), and Stavast et al. (2006); n.a. = not analyzed

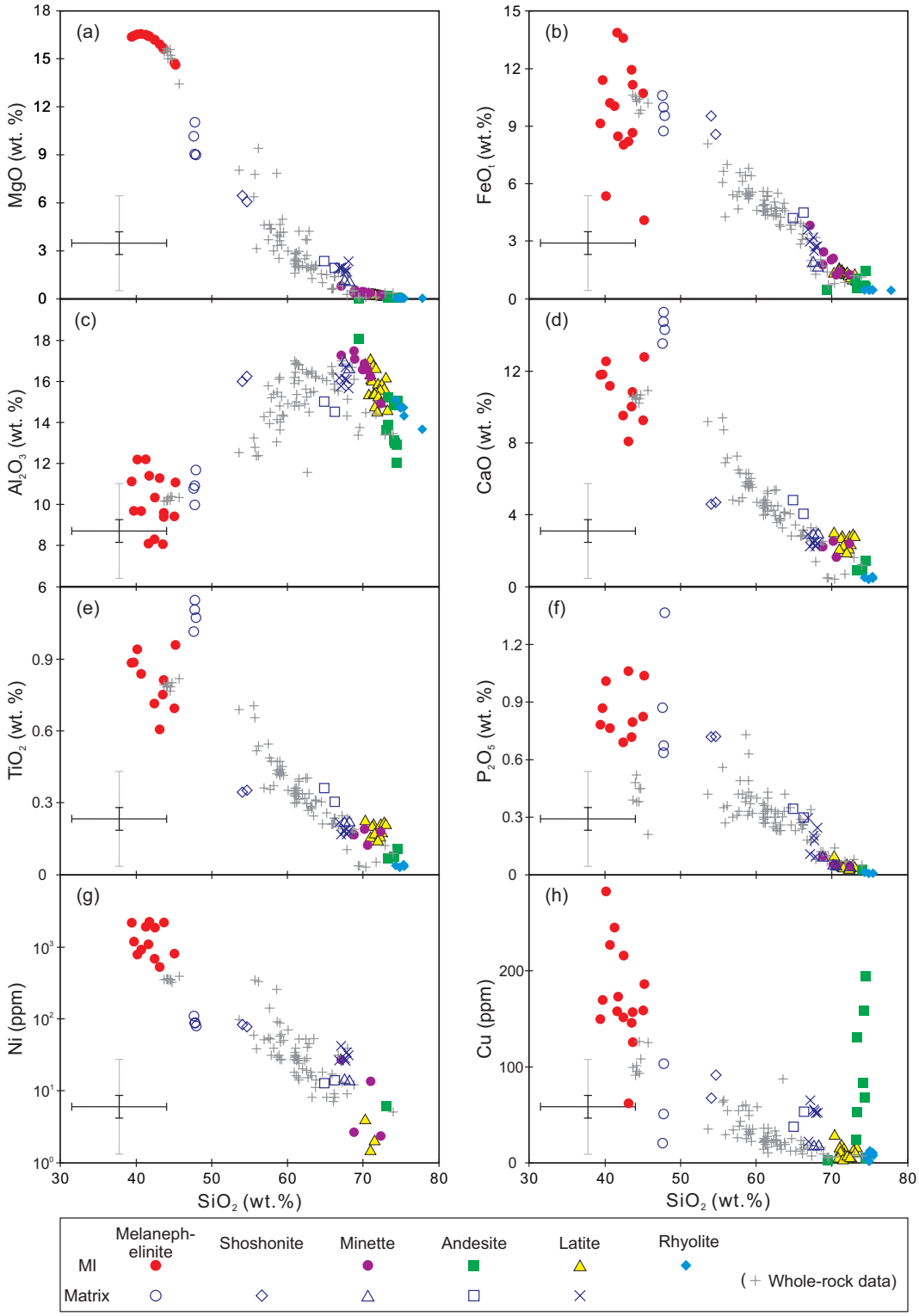

Fig. 5. Selected Harker diagrams for the Bingham magma system. Whole-rock data are shown as small, gray crosses and were taken from Maughan et al. (2002), Waite et al. (1997), Biek (2006), and Stavast et al. (2006); LA-ICP-MS analyses of melt inclusions are shown as filled symbols; LA-ICP-MS analyses of fine-grained rock matrices are shown as open symbols. The horizontal error bar in the lower left of each panel indicates the estimated uncertainty in the calculated SiO_2 content of the melt inclusions. The uncertainty in the vertical axis depends on the melt SiO_2 content and the nature of the host mineral: for melt inclusions with >60 wt % SiO_2, it is relatively small (solid line), whereas for melt inclusions with <60 wt % SiO_2, it can reach a size similar to that of the horizontal error bar (gray line). The curved arrangement of the melt inclusion data from melanephelinite in the MgO vs. SiO_2 diagram is an artifact caused by the polynomial fit through whole-rock data that was used to recalculate the LA-ICP-MS data.

similar to that of the rock matrix is indicated. The Cu content of the melt inclusion (140 ppm) is only slightly lower than that of melt inclusions analyzed from the sulfide-undersaturated melanephelinite, suggesting that, at the time of melt entrapment, the shoshonite magma either had not reached sulfide saturation yet or did so only shortly before.

From the pyroxene-bearing latite, only melt inclusions hosted by plagioclase could be quantified with a satisfactory degree of certainty. The results suggest that the trapped melts contained 67 to 72 wt % SiO_2, 0.2 to 0.8 wt % MgO, 1.6 to 2.5 wt % CaO, and 1.2 to 3.8 wt % FeO. These compositions are slightly more evolved than the fine-grained rock matrix (68 wt % SiO_2) but distinctly more evolved than the composition of the bulk rock (59 wt % SiO_2, according to LA-ICP-MS analyses on a densely pressed powder pellet). The Cu content of the plagioclase-hosted melt inclusions is extremely variable and ranges from 120 to 1,500 ppm (Fig. 5h; average 900 ppm), with most values being an order of magnitude higher than the Cu content of otherwise compositionally similar melt inclusions analyzed from other phenocryst phases in sulfide-saturated rocks investigated in this study. Similar observations have been made in melt inclusion studies performed on the Alumbrera porphyry Cu-Au deposit (Halter et al., 2005) and on a basaltic andesite from the Villarrica volcano, Chile (Zajacz and Halter, 2009). In both cases, plagioclase-hosted melt inclusions were found to contain up to an order of magnitude higher Cu concentrations than melt inclusions in other coprecipitated minerals. Whereas Halter et al. (2005) and Zajacz and Halter (2007) attributed the anomalously high Cu contents to accidental entrapment of a Cu-rich fluid phase, we prefer an explanation via postentrapment diffusional gain of Cu through plagioclase, which process could recently be reproduced experimentally (Zhang and Audétat, 2016).

In the latite samples from Castro Gulch, only plagioclase-hosted melt inclusions were analyzed because amphibole-hosted ones are very small and difficult to quantify due to the compositional similarity between host and melt, and because other phenocryst phases are either scarce (<1 vol % clinopyroxene) or altered (olivine). Consequently, only the felsic end member involved in the formation of this mixed magma was constrained. The felsic melt inclusions contain 70 to 73 wt % SiO_2, 15 to 17 wt % Al_2O_3, 3.1 to 4.8 wt % K_2O, 3.7 to 4.6 wt % Na_2O, 1.0 to 1.5 wt % FeO, and 0.2 to 0.4 wt % MgO. Copper concentrations are fairly reproducible and correlate with Sr, with most values ranging between 6 and 16 ppm.

In the Step Mountain Andesite, reliable analyses were obtained only from melt inclusions hosted by plagioclase and quartz. The results suggest that the trapped melts contain 69 to 75 wt % SiO_2, 0.5 to 1.5 wt % FeO, and 0.04 to 0.28 wt % MgO. Copper contents in the quartz-hosted melt inclusions range from 5 to 30 ppm and correlate positively with Ba (i.e., Cu contents decrease with increasing degree of melt fractionation), whereas plagioclase-hosted melt inclusions have highly variable Cu contents between 3 and 190 ppm that correlate with neither the degree of melt fractionation nor the abundance of other chalcophile elements, again suggesting postentrapment modification of original Cu contents (Fig. 5h).

Quartz-hosted melt inclusions from the Shaggy Peak Rhyolite have a rhyolitic composition and contain mostly between 7 and 14 ppm Cu (Fig. 5h, supplementary Table S2).

Composition of sulfide inclusions

Sulfide inclusions within phenocrysts are present in all investigated rock types except for the melanephelinite and the Shaggy Peak Rhyolite. In all samples, the sulfides consist dominantly of FeS, with Cu contents ranging from 1.4 to 3.5 wt % and nickel contents from 0.4 to 1.8 wt % (Table 4; supplementary Table S3). In addition, the sulfides typically contain the following concentrations of trace elements: 1,500 to 2,200 ppm Co, 200 to 500 ppm Mn, 50 to 200 ppm Zn, 30 to 60 ppm Se, 3 to 10 ppm Pb, 3 to 7 ppm Ag, 2 to 5 ppm Mo, 2 to 4 ppm Te, 0.9 to 1.8 ppm Pd, 0.3 to 0.9 ppm Bi, and 0.2 to 0.5 ppm Au. Based on reconstructed magma temperatures and Fe-Cu-S and Fe-Ni-S diagrams published by Kullerud et al. (1969), it is evident that all sulfides were trapped in the form of monosulfide solid solution.

Decomposed sulfides in the matrix of the latite consist of fine-grained clusters composed of ~50 vol % magnetite, with or without minor amounts of pyrite and/or chalcopyrite (Fig. 4d). For LA-ICP-MS analysis, we chose slightly exposed clusters, drilled them out of the surrounding matrix, and integrated the resulting signals. The signals were quantified using Fe as an internal standard, assuming that Fe behaved conservatively during the alteration of the sulfides. This assumption seems realistic if one considers the volume percentage of magnetite (~50 vol %) and the densities of pyrrhotite (4.6 g/cm^3), magnetite (5.2 g/cm^3), and matrix (~2.8 g/cm^3). The results suggest that also Ni, Co, Ag, Cd, Pd, and Pt behaved quite conservatively, whereas S, Cu, Se, Te, and Au were lost and Mn, Zn, Pb, Mo, As, Bi, and Tl were gained during the alteration process (Fig. 6).

Volatile content of rehomogenized melt inclusions in melanephelinite

About 20 olivine-hosted melt inclusions from the melanephelinite were selected for rehomogenization. Melt inclusion-bearing olivine chips were individually wrapped in Pt foil of 0.03-mm thickness and then held for 48 h at 1,100°C and 1.5-kbar confining Ar pressure in a TZM cold-seal pressure vessel.

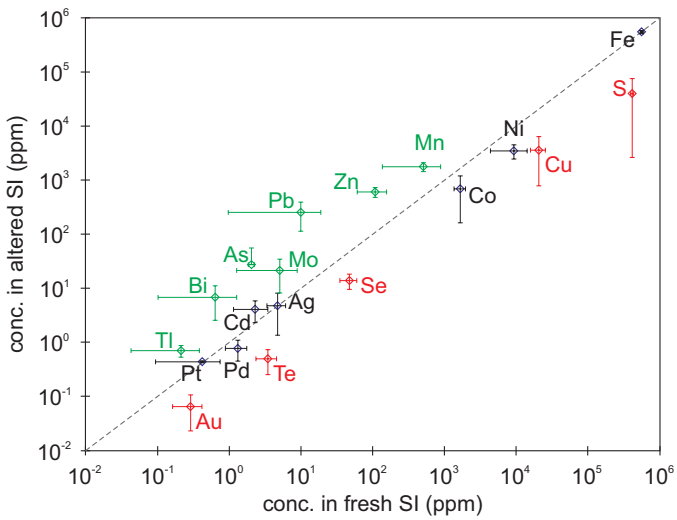

Fig. 6. Comparison of the metal and sulfur content of fresh versus altered sulfide blebs in the latite. The sulfides lost S, Cu, Se, Te, and Au but gained Mn, Zn, Pb, As, Bi, and Tl during the alteration process. SI = sulfide inclusions.

Table 4. Representative Compositions of Sulfide Inclusions Analyzed by LA-ICP-MS

	Major elements (wt %)					Trace elements (ppm)															
Sample name	S	Mn	Fe	Ni	Cu	Mg	Al	Co	Zn	As	Se	Mo	Pd	Ag	Cd	Sb	Te	Pt	Au	Tl	Pb	Bi
Shoshonite																						
Bing4 SIcpx2 13 μm	38	0.07	57	1.8	3.5	<47	<69	2,300	94	<8	<76	<5	3	7	<7.5	<2.9	<11	n.a.	<0.9	<0.7	4	1
Bing4 SIcpx4 16 μm	39	0.07	56	1.7	3.5	<44	<58	2,200	64	<4	47	<4	<3.4	5	4	<1.9	<4.0	n.a.	<0.7	<0.6	1	<1.2
Bing4 SIcpx5 16 μm	41	0.01	57	1	1.4	<24	<36	1,700	77	<3	35	24	<2.2	3	<3.9	<1.4	4	n.a.	<0.5	<0.3	7	1
Bing4 SIcpx7	38	0.08	60	0.9	1.4	<100	<98	1,700	130	<7	<92	<5	<3.5	<2.6	<11	<3.3	<9.3	n.a.	<1.4	<1.2	<5	<1.7
Pyroxene-Latite																						
Bing19 SIcpx4 8 μm	40	<0.01	56	0.7	2.9	<120	<210	2,200	17	<25	<170	<10	<5.1	<5.2	<29	<9.0	<19	n.a.	<1.1	<1.9	<9	<3.4
Bing19 SIcpx5 5 μm	40	0.19	56	0.9	3	<300	<400	2,000	270	<21	<180	<15	<12.0	<7.6	<10	<7.9	<24	n.a.	<2.2	<2.5	8	<4.9
Bing19 SIcpx5 7 μm	40	0.04	56	1.3	2.9	410	<120	2,100	33	<12	<110	<9	<7.0	<4.5	<6.1	<4.7	<14	n.a.	<1.3	<1.5	<4	<2.9
Andesite																						
Bing6 SI2hbl3 10 μm	42	0.02	55	1.2	2.8	<110	<120	2,300	150	<9	<150	<9	<5.8	4	<14	<4.8	<11	n.a.	<1.3	<0.8	6	<2.9
Bing6 SI1hbl4 15 μm	39	<0.00	57	1.4	2.4	<49	<110	2,200	<41	<10	<120	<8	<4.7	<3.0	<11	<3.5	<13	n.a.	<1.0	<1.5	<6	<2.0
Bing6 SI2hbl4 15 μm	41	<0.00	56	1.1	2.6	<39	<85	2,200	<33	<8	52	<6	<3.8	3	<8.9	<2.8	<10	n.a.	<0.8	<1.2	<5	<1.6
Bing6 SIhbl5 18 μm	40	<0.00	58	0.3	1.8	<230	<160	1,300	35	<13	<150	<11	<3.7	<5.6	<17	<4.4	<14	n.a.	<1.9	<1.5	<7	<1.8
Latite																						
Bing12 SIplag4 20 μm	39	0.05	57	0.9	3	740	<130	1,400	82	<13	<170	17	<6.9	6	<12	<4.7	<20	n.a.	<1.4	<1.4	20	<2.3
Bing12 SIhbl3 18 μm	42	0.14	54	0.6	2.8	<43	<59	1,300	240	<4	52	10	<3.6	6	<9.4	<1.9	<7.7	n.a.	<2.2	<0.7	10	1
Bing13 SIhbl4 26 μm	41	0.01	55	1.5	2.1	<14	<21	1,500	110	<2	64	5	<1.2	5	<2.3	<0.7	4	n.a.	1	<0.3	8	<0.4
Bing13 SI1hbl7 28 μm	39	<0.00	58	1.1	1.9	<14	<20	1,500	60	<2	48	5	<0.9	4	1	<0.7	3	n.a.	1	<0.1	3	0
Bing13 SIhbl9 25 μm	41	<0.00	57	0.3	2	<9	<21	1,400	95	<2	15	6	<1.4	4	<1.7	<0.5	<5.9	n.a.	0	<0.3	3	0
Bing13 SI1hbl11 40 μm	42	<0.00	54	1.5	1.9	<8	<11	2,000	69	<1	46	2	1	3	<1.1	<0.3	3	n.a.	0	<0.1	3	<0.2
Bing13 SI2hbl11 40 μm	42	<0.00	54	1.5	2.6	<6	<6	1,900	51	<1	51	2	1	3	<0.7	<0.2	2	n.a.	0	0	3	0
Bing14 SI1hbl4 23 μm	38	<0.00	59	0.4	2.2	<40	<62	1,700	<24	<6	53	<5	<4.2	4	<3.2	<1.6	<10	n.a.	<2.5	<1.3	11	1
Bing14 SI2hbl4 25 μm	40	<0.00	58	0.4	1.9	<51	<38	1,800	<13	<4	35	3	<2.5	4	<2.4	<1.7	<8.3	n.a.	<0.6	<0.5	<2	<0.8
Bing13 SIhbl 30 μm	45	n.a.	53	0.7	1.9	n.a.	n.a.	n.a.	120	<4	n.a.	n.a.	1	4	n.a.	n.a.	n.a.	0	0	n.a.	3	0
Bing13 SIhbl 30 μm	46	n.a.	50	1.6	2.6	n.a.	n.a.	n.a.	<13	<2	n.a.	n.a.	2	5	n.a.	n.a.	n.a.	1	0	n.a.	<1	<1.1
Bing13 alteredSI2matrix 70 μm	1.0	0.20	56	0.4	0.5	<16	<24	230	740	4	<23	24	1	2	<2.6	<0.9	<4.5	0	<0.4	1	280	7
Bing13 alteredSI3matrix 70 μm	5.4	0.14	56	0.4	0.3	<9	<11	1,240	570	17	15	42	0	5	5	1	<1.7	<0.3	0	1	120	4
Bing13 alteredSI4matrix 70 μm	3.8	0.15	56	0.4	0.8	<7	<8	700	440	44	9	21	1	10	5	1	0	0	0	1	480	13

Abbreviations: cpx = clinopyroxene, hbl = hornblende, n.a. = not analyzed, plag = plagioclase

Likely due to postentrapment loss of H_2O from the melt inclusions (see below), only five of them reached a mostly molten state during this process (Fig. 7). Of those, one inclusion was subsequently lost during polishing. Electron microprobe analyses of the remaining four melt inclusions (hosted in four separate olivine grains) reveal that even these inclusions did not reach full homogenization because they contain far less MgO (6.07–6.58 wt %) than the whole rock (~15.6 wt % MgO) and the calculated composition of unheated melt inclusions analyzed by LA-ICP-MS (~16 wt % MgO). For this reason, we numerically added olivine host to the electron probe microanalysis (EPMA) data until the MgO contents reached a value of 16.0 wt %. This was met after adding 24 to 25 wt % olivine (supplementary Table S4). Resulting concentrations of SiO_2 (39–42 wt %), CaO (10–11 wt %), FeO_t (9.2–10 wt %), Al_2O_3 (8.9–9.9 wt %), Na_2O (4.2–6.8 wt %), and K_2O (3.9–4.6 wt %) agree well with the range of values obtained by LA-ICP-MS on unheated melt inclusions, verifying this approach. Corresponding volatile concentrations (after dilution with olivine) are 800 to 2,500 ppm S, 3,300 to 6,900 ppm F, 2,100 to 2,600 ppm Cl, and (based on EPMA totals) 1 to 5 wt % H_2O (Table 5, supplementary Table S4). The low water content of three out of the four analyzed inclusions is not compatible with the presence of relatively H_2O rich but F- and Cl-poor phlogopite (Maughan et al., 2002). It suggests that the melt inclusions lost significant amounts of H_2O after their formation, which is also indicated by the difficulty of rehomogenizing them.

Although Maughan et al. (2002) report the existence of barite inclusions within olivine phenocrysts, we were not able to find such inclusions despite an extensive search. Therefore, in the absence of any other sulfur-, chlorine-, and fluorine-rich solid phases, the concentrations of S, Cl, and F measured in the melt inclusions can be considered a first-order approximation of their abundance in the bulk melanephelinite magma.

Discussion

Fractional crystallization vs. magma mixing

Several lines of evidence suggest that magma mixing played an important role in the formation of the ore-related latite and other intermediate magmas at Bingham Canyon: (1) whole-rock compositions defining linear trends in Harker diagrams (Fig. 5), (2) common occurrence of reversely zoned and/or compositionally distinct groups of phenocrysts, (3) occurrence of reaction rims around phenocrysts, (4) sieve-textured plagioclase, (5) the presence of melt inclusions that have a more evolved composition than the rock matrix, and (6) variable initial Sr and Nd isotope ratios that fall on a mixing array between melanephelinite and dacite (Maughan et al., 2002). Linear trends between mafic and intermediate whole-rock

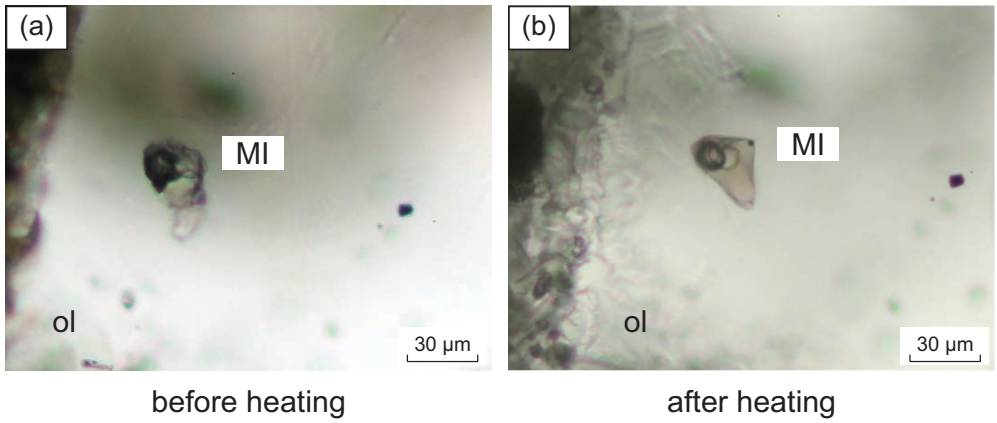

Fig. 7. Transmitted-light photomicrographs of an olivine (ol)-hosted melt inclusion (MI) from melanephelinite before (a) and after (b) rehomogenization for 48 h at 1,100°C and 1.5-kbar confining Ar pressure.

Table 5. Representative EPMA Analyses of Rehomogenized Melt Inclusions

Sample no.	Rock type	Spot	F	Na_2O	Cl	SO_3	FeO	SiO_2	MgO	K_2O	CaO	MnO	Al_2O_3	TiO_2	Total
Bingham Canyon (after numerical addition of 24–25 wt % olivine)															
Bing1	Melanephelinite	C1-3 (3 µm)	0.34	6.28	0.21	0.22	9.07	41.5	16.0	4.51	10.1	0.16	9.71	0.84	99.1
Bing1	Melanephelinite	D (3 µm)	0.62	5.59	0.26	0.38	9.89	39.9	16.0	4.31	10.2	0.13	9.47	1.14	98.1
Bing1	Melanephelinite	C2 (10 µm)	0.55	6.86	0.24	0.38	9.47	38.2	16.0	4.12	10.9	0.12	8.94	1.10	97.1
Bing1	Melanephelinite	29-MI2-2 (3 µm)	0.69	5.34	0.21	0.63	9.38	39.9	16.0	4.02	9.3	0.13	8.22	0.86	94.7
Santa Rita (no host addition)															
SR26	Basaltic andesite	45 (10 µm)	b.d.	4.57	0.03	0.05	2.73	58.5	1.12	4.82	5.05	0.09	20.0	0.87	97.8
SR26	Basaltic andesite	61 (3 µm)	b.d.	4.02	0.05	0.08	4.33	59.7	1.86	5.87	3.98	0.15	17.5	0.97	98.5
SR31	Basaltic andesite	41 (10 µm)	0.01	4.04	0.05	0.04	5.35	56.0	2.88	5.74	5.33	0.13	17.5	1.07	98.1
SR31	Basaltic andesite	42 (10 µm)	b.d.	4.02	0.05	0.04	5.49	55.2	2.84	5.79	4.97	0.13	17.5	1.18	97.2

b.d. = below detection

compositions in CaO vs. SiO_2 and MgO vs. SiO_2 diagrams are particularly indicative of magma mixing as, during closed-system fractional crystallization of mafic arc magmas, CaO and MgO rapidly decrease with increasing SiO_2 (e.g., Cassidy et al., 2015). Based on whole-rock abundances of major and trace elements, Waite et al. (1997) modeled the composition of ore-related latites as a mixture of ~10 wt % melanephelinite and ~90 wt % of a "more felsic" magma of dacitic (?) composition. However, because most of the melt inclusions analyzed from latite turned out to have a rhyolitic composition (Table 3; supplementary Table S2), we prefer a model that involves a rhyolitic end member. In this case, the composition of the latite can be approximated by a mixture of 30 to 50 wt % melanephelinite magma and 50 to 70 wt % rhyolitic magma (Figs. 5, 8a; supplementary Fig. S2).

Metal content of the latite magma

Stavast et al. (2006) conducted a detailed study on the same latite sill that was sampled in the present work. They discovered a margin that was quenched so rapidly that even most of the matrix-hosted sulfides were preserved. Based on petrographic mapping and electron microprobe maps, they estimated the abundance of sulfides in this sample at 0.19 ± 0.1 vol %, which translates to 0.30 to 0.33 wt % if one considers the density contrast between pyrrhotite and latite. Combining this sulfide content with the concentrations of strongly chalcophile elements measured by LA-ICP-MS in the sulfide inclusions (2.1 ± 0.5 wt % Cu, 1.3 ± 0.5 ppm Pd, 0.29 ± 0.13 ppm Au, 0.4 ± 0.2 ppm Pt; Table 4; supplementary Table S3) suggests that the bulk magma contained at least 50 to 80 ppm Cu, 3 to 6 ppb Pd, 0.5 to 1.3 ppb Au, and 0.6 to 1.9 ppb Pt. In the case of Pd and Pt, these minimum values should correspond to actual values because $D^{MSS/melt}$ partition coefficients are extremely high (≥6,000 for Pt, ≥44,000 for Pd; Bell et al., 2009) and the platinum group element (PGE) content of silicate and common oxide minerals is essentially nil; hence, ≥97% of these two elements were hosted in the monosulfide solid solution (MSS). In the case of Cu and Au, however, $D^{MSS/melt}$ values are significantly lower (~3,000 for Cu; ~300 for Au; Li and Audétat, 2015); hence, the amount of metal stored in the silicate melt and in minerals must also be considered. Using (1) the abovementioned $D^{MSS/melt}$ values for Cu and Au, (2) a crystal:melt ratio of 1:1 (Table 1), and (3) an average $D_{Cu}^{mineral/melt}$ value of 0.15 (Liu et al., 2014), the bulk magma can be estimated to have contained 50 to 90 ppm Cu and 0.8 to 2.0 ppb Au (Table 6). The combined values (50–90 ppm Cu, 3–6 ppb Pd, 0.8–2.0 ppb Au, and 0.6–1.9 ppb Pt) agree reasonably well with the maximum concentrations of these elements found in glassy sill margins analyzed by Stavast et al. (2006) (35 ppm Cu, 0.6 ppb Pd, 1.2 ppb Au, 0.6 ppb Pt), except for Pd, which differs by a factor of 5 to 10. The reason for the latter discrepancy is not clear. In any case, the latite bulk magma should have contained no more than 90 ppm Cu and 2.0 ppb Au.

An independent estimate of the amount of Cu present in the latite bulk magma can be obtained from magma mixing considerations. As discussed above, the ore-related latite magma can be modeled by a mixture of ~40 wt % melanephelinite magma and ~60 wt % rhyolite magma, and the composition of the melanephelinite magma can be approximated by the composition of the olivine-hosted melt inclusions. Because the melanephelinite magma was sulfide undersaturated and rhyolitic magmas are generally Cu poor (e.g., Keith et al., 1997; Johnson et al., 2013), the Cu content of the magma mixture can be approximated by taking the average Cu content of the olivine-hosted melt inclusions (180 ± 50 ppm) and mixing it at a 40:60 ratio with the average Cu content of rhyolitic melt inclusions (11 ± 6 ppm Cu, supplementary Table S2). The resulting Cu content of 79 ± 20 ppm agrees rather well with the value of 50 to 90 ppm estimated above, based on the modal abundance and composition of magmatic sulfides.

In a similar fashion, a rough estimate of the Au, Pd, and Pt content of the latite magma can be obtained by taking the concentrations of these elements in the melanephelinite whole rocks (Maughan et al., 2002) and multiplying them with a factor of 0.4 (i.e., the concentration of these elements in rhyolite is assumed to be zero). Given the crude nature of this approach, the results (3.1 ± 0.8 ppb Pd; 0.6 ± 0.2 ppb Au; 2.8 ± 0.5 ppb Pt) are in surprisingly good agreement with the estimates made based on the actual abundance and composition of sulfides in the latite magma (3–6 ppb Pd, 0.8–2.0 ppb Au, 0.6–1.9 ppb Pt). A different approach needs to be used for molybdenum because it behaves incompatibly during fractional crystallization, causing residual felsic melts to become enriched in Mo (e.g., Audétat, 2010, 2015). Hence, the contribution from the felsic end member needs to be taken into account. Based on Mo contents of 1 to 3 ppm in melanephelinitic melt inclusions, 2 to 3 ppm in rhyolitic melt inclusions,

Table 6. Mass Balance Constraints for the Metal Content of Latite

	Cu	Pd	Au	Pt
Concentration in sulfide (ppm)	21,000 ± 500	1.3 ± 0.5	0.29 ± 0.13	0.4 ± 0.2
Melt (wt %)	50	50	50	50
$D_{MSS/SM}$[1]	3,000	44,000	300	6,000
Calculated concentration in melt[2]	7 ± 2	0.03 ± 0.01	1.0 ± 0.4	0.07 ± 0.03
Crystals (wt %)	50	50	50	50
Calculated concentration in crystals[3]	1.0 ± 0.3	–	–	–
Calculated concentration in whole rock[4]	53–87	2.5–5.7	0.8–2.0	0.6–1.9
% metals stored in sulfide	94	99.6	65	97

[1] $D_{MSS/SM}$ values are from Bell et al. (2009; Pd and Pt) and Li and Audétat (2015; Cu and Au)
[2] Copper concentration is given in ppm; concentrations of the other metals are given in ppb
[3] Cu content of crystals was calculated based on an average bulk crystal/melt partition coefficient of 0.15 reported in Liu et al. (2014, 2015)
[4] Based on a sulfide abundance of 0.30 to 0.33; copper concentration is given in ppm; concentrations of the other metals are given in ppb

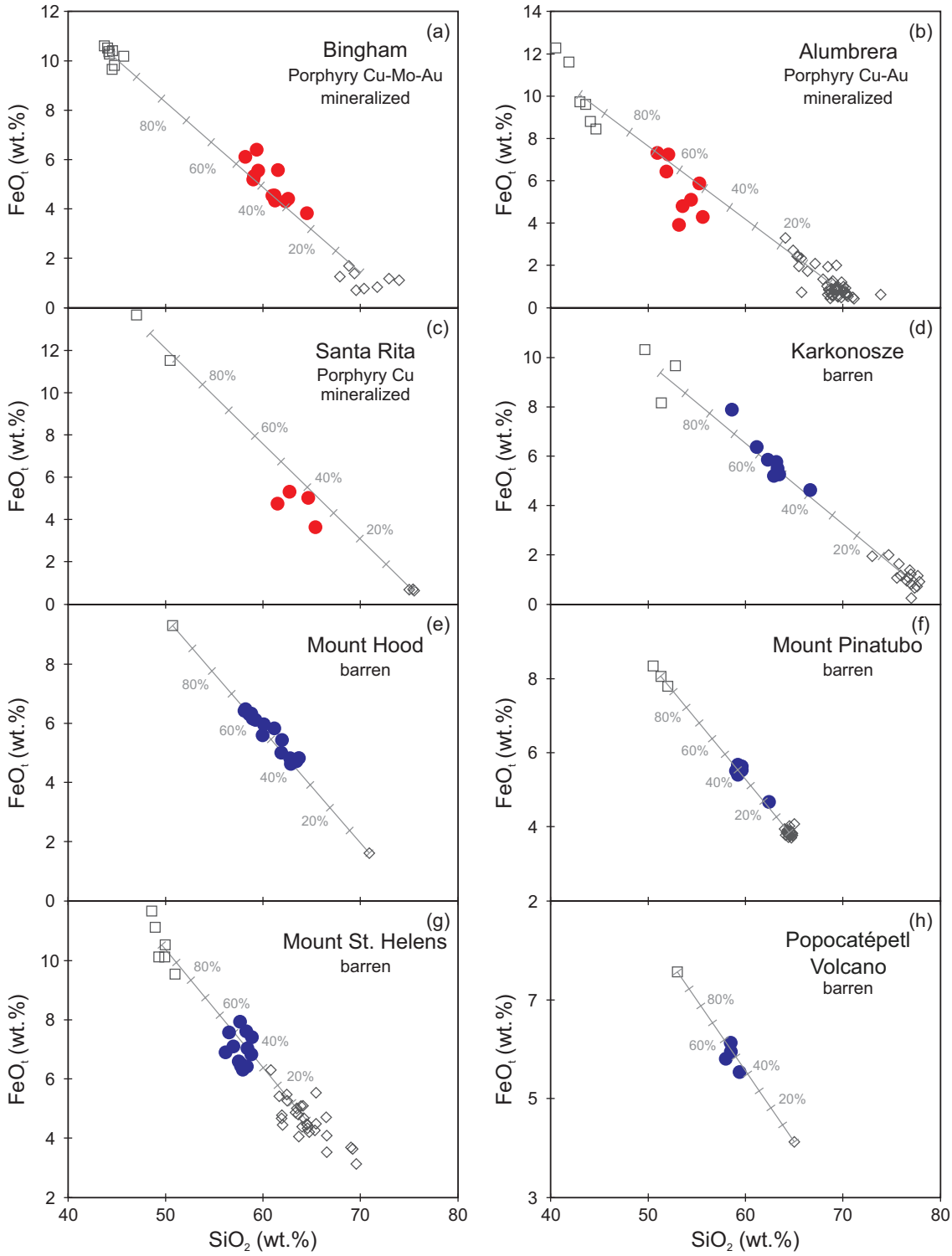

Fig. 8. FeO vs. SiO_2 diagrams depicting whole-rock data and melt inclusion compositions from three porphyry Cu deposits and five barren arc magma systems. In all cases, the most mafic and most felsic magma compositions are shown, plus the compositions of typical intermediate members. The fact that the latter plot on linear interpolations between the two end members suggests that they formed by magma mixing rather than by fractional crystallization, as the latter process results in FeO vs. SiO_2 trends that are strongly curved downward. Tick marks and associated numbers refer to percentages of mafic end member involved in hypothetical mixing trends. Data sources: Bingham—whole-rock data (same sources as in Fig. 5); Alumbrera—melt inclusion data from Halter et al. (2004b); Santa Rita—whole-rock data from Jones et al. (1967) and this study, plus melt inclusion data from Audétat and Pettke (2006). Sources of whole-rock data used for barren magma systems: Karkonosze—Słaby and Martin (2008); Mount Hood—Kent et al. (2010); Mount Pinatubo—Pallister et al. (1996); Mount St. Helens—Smith and Leeman (1987, 1993); Popocatépetl volcano—Witter et al. (2005).

and a mafic to felsic magma mixing ratio of ~40:60, the Mo content of the latite bulk magma can be estimated at 2 to 3 ppm Mo.

Temporary storage of chalcophile elements in magmatic sulfides

Although magmatic sulfides take up large amounts of chalcophile elements, attainment of sulfide saturation in upper-crustal magma chambers does not necessarily have a negative effect on the mineralization potential: petrographic studies have shown that magmatic sulfides in upper-crustal intrusives usually get destroyed at late-magmatic to subsolidus stages (except for sulfide droplets that are fully enclosed within other minerals); hence, most of the metal taken up by magmatic sulfides becomes available for the mineralizing fluids (e.g., Keith et al., 1997; Larocque et al., 2000; Audétat and Pettke, 2006; Stavast et al., 2006; Nadeau et al., 2010; Audétat and Simon, 2012). That chalcophile elements are only temporarily stored in magmatic sulfides at upper-crustal levels is also indicated by reports of matching metal ratios in magmatic sulfides vs. premineralization fluid inclusions, volcanic gases, and/or bulk ores (Halter et al., 2005; Stavast et al., 2006, Nadeau et al., 2010). In the case of Bingham Canyon, Stavast et al. (2006) found that the relative proportions of S, Cu, Mo, Au, and Pb lost from the slowly cooled latite sill interior are similar to those present in the bulk mineralization. A similar comparison can now be made based on the LA-ICP-MS analyses of sulfide inclusions (Fig. 9). Whereas S:Cu:Au:Ag ratios in the magmatic sulfides match well with those in the bulk ore, the relative abundances of Mo, Zn, and Pb in the magmatic sulfides are distinctly lower. This observation agrees with the fact that $D^{MSS/melt}$ values of Mo, Zn, and Pb are orders of magnitude lower than those of S, Cu, Au, and Ag (Li and Audétat, 2012, 2015), meaning that only insignificant amounts of Mo, Zn, and Pb are sequestered by the magmatic sulfides. Metal ratios in premineralization, intermediate-density fluid inclusions at Bingham Canyon (Landtwing et al., 2010; Seo et al., 2012) match those of magmatic sulfides only with regard to Cu:Ag, whereas the relative abundances of Mo, Pb, and Zn in the fluid inclusions more closely resemble those of the bulk ore (Fig. 9). Interestingly, the Au:Cu ratio of the fluid inclusions is distinctly higher than that of both the magmatic sulfides and the bulk ore. The reason for this discrepancy is not clear, but, potentially, it reflects preferential transport of Au to the epithermal environment (Heinrich et al., 2004), leading to a lower Au:Cu ratio at the level of the porphyry deposit.

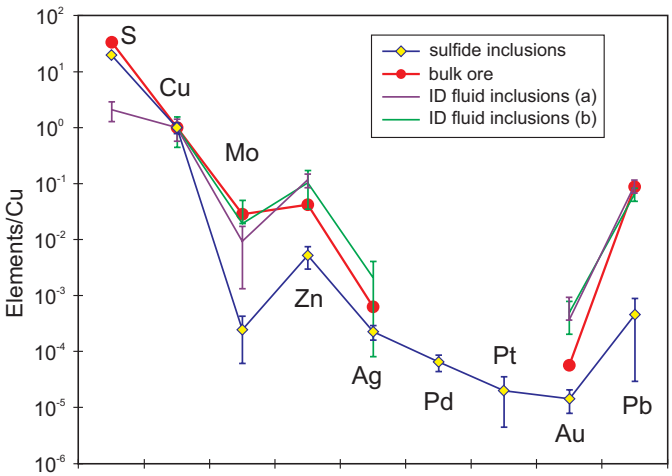

Fig. 9. Element ratios (normalized to Cu) in well-preserved sulfide inclusions compared to those of the bulk ore at Bingham Canyon. Also shown are element ratios in intermediate density (ID) fluid inclusions reported by Seo et al. (2012: a) and Landtwing et al. (2010: b). The sulfide inclusions have an S:Cu:Ag:Au ratio similar to that of the bulk ore but contain less Mo, Zn, and Pb, which is explained by the lower sulfide/melt partition coefficients of the latter elements. The intermediate-density fluid inclusions have element ratios similar to those of the bulk ore, except for lower S and higher Au. Data sources for the bulk ore as follows: metal ratios are from Mutschler et al. (1999); sulfur content is from Hattori and Keith (2001).

Comparison with other magma systems

In order to identify potential key factors in the genesis of porphyry Cu (±Mo, Au) deposits, we will now compare the results discussed above with data from two other mineralized magma systems (Santa Rita, USA, Audétat and Pettke, 2006; Alumbrera, Argentina, Halter et al., 2005) and several presumably barren arc magma systems. As barren systems, we chose modern arc volcanoes, which means that we do not know whether these magma systems ultimately will be barren or mineralized. However, as economically mineralized magma systems are generally rare, it appears safe to assume that most of the chosen modern occurrences will ultimately be barren. Both the two additional porphyry Cu-mineralized occurrences and the modern arc volcanoes were chosen based on evidence for magma mixing and the availability of data regarding the metal and volatile content of mafic input magmas, such that metal and volatile content of intermediate magmas can be estimated indirectly using the approach outlined above. At Santa Rita, the age relationship between the studied mafic samples (one corresponding to the most mafic sample described in Audétat and Pettke, 2006, and one collected more recently from an even more mafic dike that was truly sulfide undersaturated) and the mineralization is not well constrained. New age data reported by Mizer et al. (2015) suggest that some of the dikes in the North Star Basin are 13 m.y. younger than the mineralization (the latter dated at 59.5 ± 1.5 Ma), whereas mineralogically similar dikes occurring 2 to 3 km farther east are crosscut by ore-related quartz monzodiorite porphyry dikes (Hernon et al., 1964; Jones et al., 1967). Other dikes in the North Star Basin appear to be related to a conspicuous layer of andesite breccia, which itself is cut by the 74.4-m.y.-old, Cu-Zn-Ag-Au–mineralized Piños Altos pluton 5 km farther west (McLemore, 2008). Hence, the investigated samples could theoretically be anywhere from ≥15 m.y. older to ≥13 m.y. younger than the mineralization at Santa Rita, but, based on the crosscutting relationships of mineralogically similar dikes with ore-related quartz monzodiorite porphyry, we believe that they are of premineralization origin.

1. Extent of mixing with mafic magma

The chemical arguments and mass balance calculations presented above suggest that the ore-related latite magma at Bingham Canyon gained most of its Cu, Au, and S from the mafic magma that was involved in the mixing event. A magma-mixing origin of intermediate magmas has been documented from several other porphyry Cu (±Mo, Au) deposits, such as Alumbrera (Halter et al., 2004b), Santa Rita (Audétat and

Pettke, 2006), Grasberg (Pollard et al., 2005), Ok Tedi (van Dongen et al., 2010), and Yanacocha (Chiaradia et al., 2009), as well as from numerous unmineralized magma systems (e.g., reviews by Eichelberger, 1978; Reubi and Blundy, 2009; Kent et al., 2010). This does not mean that magma mixing is a requirement for economic mineralization, as there are also examples of porphyry Cu (±Mo, Au)–mineralized magma systems that show no or only little evidence for magma mixing, such as Yerington (Dilles, 1987) and the Highland Valley deposits (McMillan, 2005). However, for the present discussion we focus on magma systems that evolved prominently by magma mixing because they allow the metal content of intermediate magmas to be estimated based on the metal content of the mafic input magma and the mixing ratio with more silicic magmas. Reconstructed compositions of the most mafic, the most felsic, and typical intermediate magmas present in three porphyry Cu (±Mo, Au)–mineralized systems and five presumably barren arc magma systems are shown in Figure 8 and the supplementary Figure S1. In all cases, the intermediate magma compositions lie on simple mixing trends as opposed to fractional crystallization trends that would be characterized by rapid decreases in Fe, Mg, and Ca between 45 and 55 wt % SiO_2. The percentage of mafic magma involved in the intermediate magmas varies from ~30% to ~70%, with no systematic difference between barren and mineralized systems. Therefore, the ore-related intermediate magmas at Bingham Canyon, Santa Rita, and Alumbrera do not seem to involve higher proportions of mafic end-member magmas than the intermediate magmas occurring in barren magma systems. However, there appears to be a trend of the mafic end members in mineralized systems being more mafic than those in barren systems (Fig. 8).

2. *Metal content of mafic input magmas*

LA-ICP-MS analyses of olivine-hosted melt inclusions from the melanephelinite at Bingham Canyon suggest that the mafic input magma contained about 150 to 280 ppm Cu (Fig. 10a; Table 3). Similar concentrations are found in mafic,

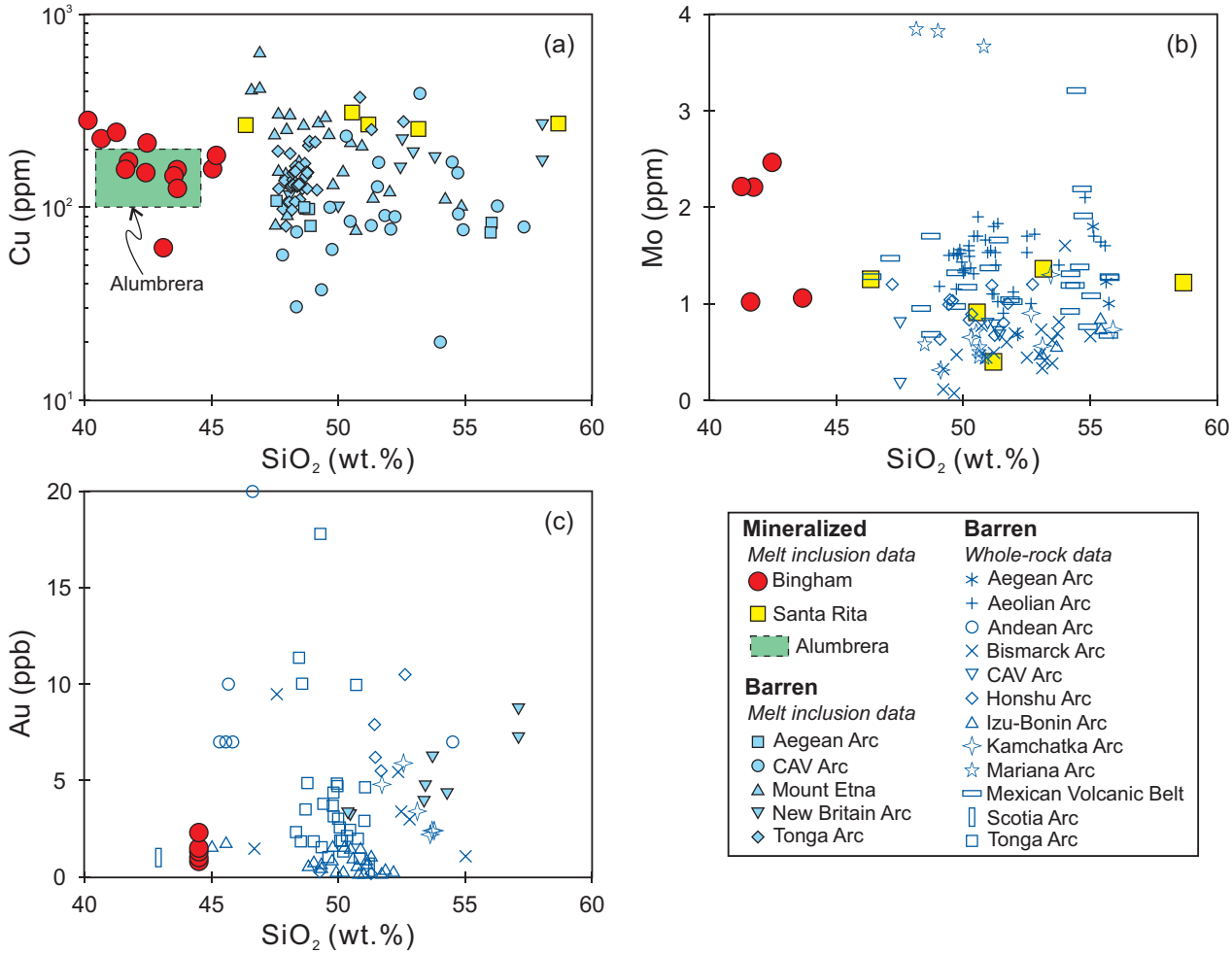

Fig. 10. Metal content of mafic melt inclusions and whole rocks in mineralized versus barren arc magma systems. Melt inclusion data from Bingham Canyon and Santa Rita are from this study and are listed in supplementary Tables S2 and S5, respectively; estimated Cu content of mafic input magma at Alumbrera is from Halter et al. (2005); Au contents of melanephelinite whole rocks from Bingham Canyon are from Maughan et al. (2002). Sources of melt inclusion data for barren arc magma systems: Aegean arc—Vaggelli et al. (2009); Central American volcanic arc (CAV)—Lloyd et al. (2013); Mount Etna—Collins et al. (2009); New Britain arc—Sun et al. (2004b); Tonga arc—Sun et al. (2004a), Leslie et al. (2009). Whole-rock data from barren systems are taken from the Geochemistry of Rocks of the Oceans and Continents (GEOROC) database.

sulfide-undersaturated melt inclusions of basaltic trachyandesite to phonotephrite composition from the Santa Rita porphyry Cu-Mo-Au deposit (260–360 ppm; Audétat and Pettke, 2006; and new, so far unpublished data provided in supplementary Table S5). The latter melt inclusion data were calculated using the Al_2O_3 content of finely crushed bulk rock of that same sample as an internal standard. For the porphyry Cu-Mo-Au deposit at Bajo de la Alumbrera, Halter et al. (2005) constrained the Cu content of the mafic, sulfide-undersaturated input magma at 100 to 200 ppm Cu.

For the presumably barren arc magma systems depicted in Figure 9, no melt inclusion data are available for the mafic end member. For this reason, we used data of olivine-hosted melt inclusions from other arc magma systems (as compiled in the GeoRoc melt inclusion database) as a reference for barren systems. The only occurrences for which data on both Cu and SiO_2 are listed in this database are the Tonga arc (Sun et al., 2004a; Leslie et al., 2009), the Aegean arc (Vaggelli et al., 2009), the Central American volcanic arc (Lloyd et al., 2013), the New Britain arc (Sun et al., 2004b), and Mt. Etna (Collins et al., 2009). The melt inclusion Cu contents from these occurrences cover a wide range, from 20 to 380 ppm, with most data points falling between 100 and 200 ppm (Fig. 10a). These data suggest that the mafic input magmas at Bingham Canyon, Santa Rita, and Alumbrera were not unusually Cu rich compared to their counterparts in barren arc magmas. However, more data are needed (especially from mineralized systems) to make firm conclusions.

A similar picture emerges with respect to Mo and Au abundances (Fig. 10b, c). In the case of Mo, few melt inclusion data are available in the GeoRoc database, for which reason we instead used data from fresh whole rocks for barren samples. Notice that metals may have been lost from these samples but are unlikely to have been added to them; hence, the data probably represent minimum values. Again, no systematic differences between barren and mineralized magma systems were noticed. In the case of Au, only whole-rock data can be compared because the Au contents of mafic melts are generally too low to be measured by LA-ICP-MS in single melt inclusions. The data shown in Figure 10c suggest that the mafic input magma at Bingham Canyon was not particularly Au rich compared to other mafic arc magmas.

In summary, the data shown in Figure 10 provide no evidence that the mafic input magmas in mineralized systems were unusually metal rich. The same conclusion was reached in a recent study on a porphyry Cu deposit in northern China (Hou et al., 2015).

3. *Sulfur content*

Hunt (1991) pointed out that porphyry Cu deposits are, first and foremost, large sulfur anomalies, with enrichment in S being 10 to 100 times greater than enrichment in Cu when compared to the abundance of these elements in average continental crust. Therefore, the possibility of a major control of magmatic sulfur contents on the mineralization potential needs to be explored. Rehomogenized melt inclusions from the melanephelinite at Bingham Canyon contain 800 to 2,500 ppm S, which is well within the range of sulfur contents reported for mafic melt inclusions in other primitive arc magmas (Fig. 11a). Therefore, the mafic input magma at Bingham Canyon does not seem to have been unusually rich in sulfur. However, the concentration of 800 to 2,500 ppm S measured in mafic melt inclusions is too low to account for the sulfur content of the latite magma (>1,300 ppm, based on a sulfide content of 0.31 wt % and the additional presence of anhydrite) if all the sulfur present in the latite magma were derived from the mafic end member. In that case, the mafic end member had to contain ≥3,000 to 3,500 ppm S (assuming ~40% mafic component in hybrid latite magma). The discrepancy can be explained by the fact that the felsic end-member magma involved in the generation of the hybrid latite magma also contained appreciable amounts of sulfur, as is shown by the presence of anhydrite inclusions in plagioclase phenocrysts with compositions similar to those hosting the rhyolitic melt inclusions (supplementary Table S6). The presence of magmatic anhydrite in the felsic end member suggests that sulfur may have been added via volatile fluxing from underlying mafic magma (Hattori, 1993; Keith et al., 1997) and, thus, that in the case of sulfur the indirect approach via the composition of mafic melt inclusions and the mafic to felsic magma mixing ratio provides only a minimum estimate of the sulfur content of the mixed magma.

The same is true for Santa Rita, where both the felsic end-member magma and the hybrid, ore-related quartz monzodiorite magma contained magmatic anhydrite (Audétat et al., 2004; Audétat and Pettke, 2006). Based on a modal abundance of 1 to 2 vol % anhydrite phenocrysts, the ore-related quartz monzodiorite magma at Santa Rita contained 2,500 to 4,000 ppm S (Audétat et al., 2004), which is far more than the ≤300 ppm S present in the analyzed mafic melt inclusions (Fig. 11). For Alumbrera, no data on volatile concentrations in melt inclusions are available, but, based on a Cu content of ~100 ppm in sulfide-undersaturated andesitic melt inclusions and an average S/Cu ratio of 40 in magmatic sulfides, Halter et al. (2005) estimated the sulfur content of the ore-forming magmas at ca. 4,000 ppm S. Chambefort et al. (2008) constrained a minimum value of 1,000 ppm S for anhydrite-saturated magmas associated with high-sulfidation epithermal Au deposits at Yanacocha, based on anhydrite solubility. Magmatic anhydrite has also been reported from the "porphyry A" stock at El Teniente (Stern et al., 2007) and from a granodiorite porphyry associated with the Qulong porphyry Cu-Mo deposit in Tibet (Xiao et al., 2012).

A quantitative comparison with barren arc magma systems is difficult because evidence for volatile fluxing and the formation of magmatic anhydrite is also common in barren systems (e.g., Luhr, 2008; Parat et al., 2011; Wallace and Edmonds, 2011). The trachyandesite of El Chichón contained ~2,500 ppm S, based on an anhydrite content of ca. 1 vol % (Luhr, 2008), whereas the Mt. Pinatubo dacite contained <2,500 ppm S (Pallister et al., 1996). No quantitative estimates are available for other intermediate magmas of "barren" systems. Therefore, we presently cannot say with any confidence whether or not porphyry Cu (±Mo, Au)–forming magmas contain more sulfur than nonmineralizing arc magmas.

4. *Water, fluorine, and chlorine contents*

Porphyry Cu (±Mo, Au)–mineralizing magmas commonly exhibit high Sr/Y ratios (Richards, 2011; Loucks, 2014), which has been interpreted by some researchers to reflect unusually

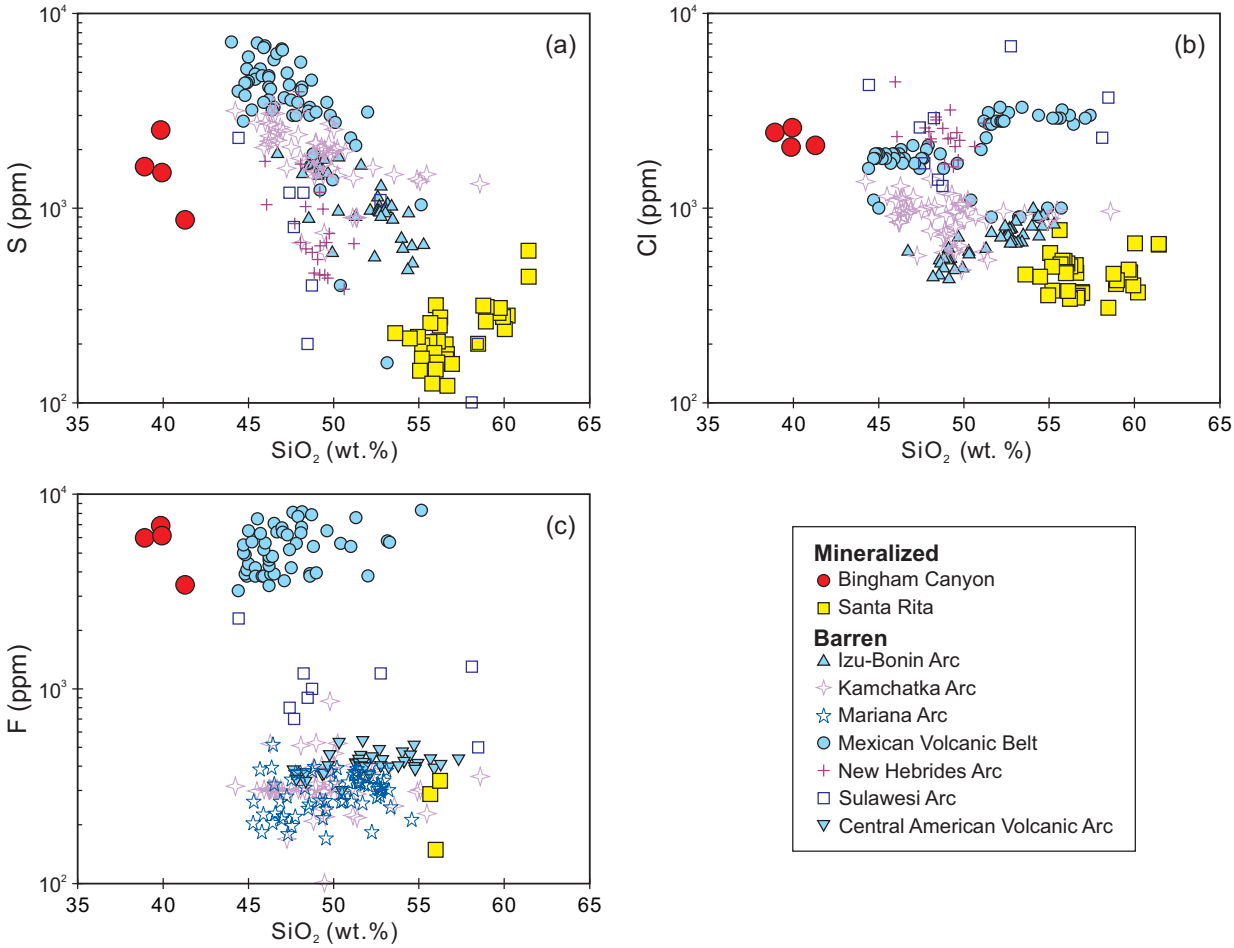

Fig. 11. Volatile content (S, F, and Cl) of mafic melt inclusions from mineralized (Bingham Canyon and Santa Rita) vs. barren arc magmas. Data sources for Bingham Canyon and Santa Rita are from this study and are listed in Table 5 and supplementary Table S4. Data sources for barren arc magmas: Izu-Bonin arc—Saito et al. (2010); Kamchatka arc—Portnyagin et al. (2007); Mariana arc—Kelley et al. (2010); Mexican volcanic belt—Vigouroux et al. (2008), Maria and Luhr (2008); New Hebrides arc—Métrich and Deloule (2014); Sulawesi arc—Elburg et al. (2006); Central American volcanic arc—Lloyd et al. (2013).

high water contents of the parental magmas (e.g., Rodríguez et al., 2007; Alonso-Perez et al., 2009; Richards, 2011). High water contents may promote the mineralization potential via more efficient metal extraction from the magma and the formation of vent structures into which fluids are focused. However, as demonstrated by Loucks (2014), high Sr/Y can also be produced from arc magmas that contain normal water concentrations if they undergo fractional crystallization at high pressure. A comprehensive treatment of this topic is beyond the scope of this contribution, but it looks like it is not possible to discriminate between these two possibilities based on trace element signatures alone. Most of the magmas present at Bingham Canyon (including the ore-related latite) were clearly hydrous, as indicated by the common presence of hornblende and biotite phenocrysts. However, whether or not they were more hydrous than ordinary arc magmas remains to be tested. Unfortunately, the water content of rehomogenized melt inclusions from the melanephelinite cannot be used as a criterion, because these inclusions seem to have lost water (see above). An experimental study performed by Irving and Green (2008) on a composition similar to the Bingham melanephelinite (their "basanite + 10 vol % olivine" mix) reproduced the assemblage olivine + phlogopite + clinopyroxene at 1,120° to 1,160°C and 10 to 20 kbar at a water content of 4.5 wt %. This water content is similar to that of primitive arc magmas in general (3.9 ± 0.4 wt % H_2O; Plank et al., 2013). The phlogopites in the melanephelinite of Bingham Canyon have a high enough molar OH/F ratio (~4.2; Maughan et al., 2002) to allow comparison with this F-free experimental system. Therefore, based on these indirect constraints, we do not see any evidence that the magmas at Bingham Canyon were unusually water rich.

The mineralization potential of magmas may also be affected by the content of other volatiles, in particular by the availability of chlorine, because this element promotes the partitioning of Cu and Au into the exsolving fluid phase (e.g., Candela and Holland, 1984; Zajacz et al., 2010). Electron microprobe analyses of rehomogenized melt inclusions from the melanephelinite at Bingham Canyon suggest fluorine and chlorine concentrations of 3,300 to 6,900 and 2,100 to 2,600 ppm, respectively. Three out of the five presumably barren arc magma systems plotted in Figure 11b show similar chlorine contents; hence,

the melanephelinite magma of Bingham Canyon does not seem to have been unusually chlorine rich. Although chlorine concentrations are likely to be affected by volatile fluxing, there is no evidence that major amounts of chlorine are stored in solid phases in intermediate to felsic magmas. However, chlorine contents of felsic melts commonly are similar to those of mafic melts (e.g., Webster, 2004; Webster et al., 2015); hence, admixture of felsic magmas does not necessarily result in lower Cl concentrations. Therefore, we believe that, in contrast to sulfur, the chlorine content of mafic input melts is a good approximation of the chlorine content of potentially mineralizing, intermediate magmas. The same applies for fluorine. Interestingly, the fluorine content of the melt inclusions analyzed from the melanephelinite at Bingham Canyon is about an order of magnitude higher than that of most data reported from barren systems. The only melt inclusions from barren systems with similarly high fluorine contents are those of potassic basanites from the Mexican volcanic belt (Fig. 11c). These magmas are interpreted to have formed by small-degree partial melting of phlogopite- and garnet-bearing peridotite that was metasomatized by slab-derived fluids (Vigouroux et al., 2008). In the case of Bingham Canyon, such an event of subduction-related metasomatism and metal enrichment in the mantle source can be traced back to the Early Proterozoic (Pettke et al., 2010). It seems unlikely, however, that the Bingham Canyon magma system became so productive due to elevated fluorine contents, as this element does not form stable complexes with Cu, Mo, and Au in hydrothermal fluids (e.g., Keppler and Wyllie, 1991), nor do fluorine contents of a few thousand ppm significantly affect magmatic phase relationships. The fluorine and chlorine contents of the mafic melt inclusions analyzed from Santa Rita are within the range displayed by most of the barren systems. Hence, there is no evidence for unusually high amounts of water, chlorine, and fluorine in the productive magma systems, except for elevated fluorine contents in the case of Bingham Canyon.

5. *Other parameters*

In view of the lack of evidence for unusually high concentrations of metals, chlorine, and water in the mafic input magmas at Bingham Canyon, Santa Rita, and Alumbrera, other factors affecting the mineralization potential of arc magmas need to be considered. One such factor is the emplacement level of the magma chamber. If the magma chamber forms at too great a depth, then it is unlikely to develop structures such as stockwork zones or breccia pipes into which magmatic-hydrothermal fluids can be focused (e.g., Cloos, 2001; Richards, 2005; Sillitoe, 2010). If the chamber forms at very shallow levels, then it is likely to erupt in a catastrophic, caldera-forming event. Due to this, porphyry Cu-mineralizing magma chambers are located almost exclusively at 5- to 15-km paleodepth (Sillitoe, 2010). However, numerous other subduction-related intrusions exposed in the North American Cordillera were emplaced at a similar depth range (2–10 km; Ducea and Barton, 2007), and it seems very unlikely that all of them were mineralized. Therefore, additional factors must be met in order to produce economic porphyry Cu mineralization.

Another potential key factor may be the size of the magma chamber. Obviously, very large amounts of magma were needed to supply all the Cu, Au, and Mo present in economic deposits if the conclusions above are correct, i.e., that the magmas were not exceptionally metal rich. Taking an average Cu content of ~70 ppm for the latite (see above) and a total endowment of 28.5 Mt Cu at Bingham Canyon (Mutschler et al., 1999), at least 150 km^3 of latite magma was required to form this deposit. Similar minimum volumes were calculated by Richards (2005) for supergiant (≥10 Mt Cu) porphyry Cu deposits in general. Assuming an average Cu content of 60 ppm in andesite magmas, he calculated that at least 100 km^3 of magma was needed to supply the amount of Cu stored in such deposits. Actual magma volumes must have been considerably higher, because neither the Cu extraction efficiency nor the Cu deposition efficiency is 100%. Based on geophysical and thermal constraints, Steinberger et al. (2013) estimated the volume of the magma chamber beneath Bingham Canyon at ~2,000 km^3. Similar magma chamber volumes are indicated by the size of exposed cogenetic plutons at the porphyry Cu deposits at Yerington, USA (~1,300 km^3; Dilles et al., 1987), and the Highland Valley porphyry cluster, Canada (≥1,000 km^3 if only the younger phases are considered; ≥5,000 km^3 if the older phases are included; McMillan, 2005). A rigorous comparison of magma chamber volumes in barren versus mineralized systems is difficult due the fact that, in mineralized systems, the underlying source magma chamber is usually not exposed, whereas in the case of large, exposed plutons, it is unclear whether or not a deposit once was present at higher levels. Furthermore, large plutons or batholiths commonly consist of multiple intrusions that were emplaced over too long a time interval to be able to interact with each other. In an attempt to make such a comparison, Cloos (2001) found that magma chambers beneath active arc volcanoes seldom exceed a volume of 100 to 200 km^3, and that special tectonic circumstances are required to produce large upper-crustal magma chambers. The same conclusion was reached by Richards (2005), who pointed out that large magma fluxes are necessary to create large upper-crustal magma chambers. However, if the mineralization potential indeed depends critically on the size of the upper-crustal magma chamber, then how does this fit with the high Sr/Y ratio of fertile magmas, which appears to be inherited from processes operating in the lower crust? It would mean that the same circumstances that cause high Sr/Y ratios also promote the formation of large magma chambers in the upper crust. Indeed, recent work by Ducea et al. (2015) suggests that high Sr/Y magmas tend to form during periods of a high magma production rate (so-called flare-up events), which themselves are associated with periods of crustal thickening. Therefore, if it is true that large magma fluxes are necessary to create large upper-crustal magma chambers, then a link to the high Sr/Y signature of fertile magmas seems feasible.

In summary, based on the few data currently available, we do not see any evidence that porphyry Cu (±Au, Mo)–forming magmas were systematically enriched in Cu, chlorine, or water compared to nonmineralizing arc magmas, nor does magma chamber depth (although certainly important) seem to be the sole factor controlling the mineralization potential. What remain from the list of potential key parameters mentioned in the introduction are (1) sulfur content and (2) magma chamber size. The former is linked to f_{O_2} and magma composition, because sulfur solubility in silicate melts strongly

increases with f_{O_2} and magma alkalinity (e.g., Jugo et al., 2010; Baker and Moretti, 2011; Masotta and Keppler, 2015), whereas the latter may be linked to tectonic regime. Further work is required to constrain the effects of these parameters on the mineralization potential of arc magmas.

Conclusions

The results of this study suggest that the ore-related latite magma at Bingham Canyon was produced by mixing of ~40 wt % mafic magma of approximately melanephelinitic composition with ~60 wt % felsic magma of rhyolitic composition. The mafic magma provided the bulk of copper and gold present in the latite, and the mixing process resulted in the precipitation of ~0.3 wt % magmatic sulfides, which sequestered nearly all available S, Cu, and Au. Sulfur appears to have been contributed from both end members, but the felsic magma probably became enriched in sulfur via fluxing of volatiles from underplating mafic magma. Based on the abundance and composition of magmatic sulfides, the ore-related latite magma at Bingham Canyon is estimated to have contained 50 to 90 ppm Cu, 0.8 to 2.0 ppb Au, 2 to 3 ppm Mo, and ≥0.12 to 0.14 wt % S. The precipitation of magmatic sulfides was not detrimental to the mineralization potential because most sulfides were subsequently destroyed (at the magmatic or subsolidus stage), and thereby released their sulfur and metal content to the mineralizing fluids. An independent, first-order estimate of the Cu content of the latite magma can be obtained by taking the average Cu content of mafic, sulfide-undersaturated melt inclusions and diluting it with the amount of admixed felsic end member.

Applying the latter approach for two other porphyry Cu-mineralized magma systems (Santa Rita, USA, and Bajo de la Alumbrera, Argentina) and several presumably barren magma systems suggests that the input magmas in mineralized systems were not unusually rich in Cu or Cl and H_2O. The situation for sulfur is unclear because major amounts of sulfur can also be provided by the felsic end member. Clearly, more data are needed to allow firm conclusions. If mineralizing magmas prove to be unusually sulfur rich, then this factor (which likely is linked to magma oxidation state and/or the extent of mafic magma underplating and associated volatile fluxing) may play a key role in the formation of porphyry Cu (±Mo, Au) deposits. If mineralizing magmas prove to have normal sulfur contents, then other parameters, such as the formation of unusually large magma chambers within 5- to 15-km depth and the development of vent structures that enable focused fluid flow, may dominate.

Acknowledgments

This study was partially financed by a China Scholarship Council grant to the first author. We would like to thank Raphael Njul for the preparation of the polished thick sections, Detlef Krauße for help with the microprobe analyses, and Brian Rusk, Adam Simon, and associate editor Jacob Hanley for their thoughtful reviews, which greatly helped to improve the manuscript.

REFERENCES

Alberico, A., Ferrando, S., Ivaldi, G., and Ferraris, G., 2003, X-ray single-crystal structure refinement of an OH-rich topaz from Sulu UHP terrane (eastern China)—structural foundation of the correlation between cell parameters and fluorine content: European Journal of Mineralogy, v. 15, p. 875–881.

Alonso-Perez, R., Müntener, O., and Ulmer, P., 2009, Igneous garnet and amphibole fractionation in the roots of island arcs: Experimental constraints on andesitic liquids: Contributions to Mineralogy and Petrology, v. 157, p. 541–558.

Andersen, D.J., and Lindsley, D.H., 1985, New (and final!) models for the Ti-magnetite/ilmenite geothermometer and oxygen barometer: Eos, Transactions, American Geophysical Union, v. 66, p. 416 (abstract).

Audétat, A., 2010, Source and evolution of molybdenum in the porphyry Mo (-Nb) deposit at Cave Peak, Texas: Journal of Petrology, v. 51, p. 1739–1760.

——2015, Compositional evolution and formation conditions of magmas and fluids related to porphyry Mo mineralization at Climax, Colorado: Journal of Petrology, v. 56, p. 1519–1546.

Audétat, A., and Pettke, T., 2006, Evolution of a porphyry-Cu mineralized magma system at Santa Rita, New Mexico (U.S.A.): Journal of Petrology, v. 47, p. 2021–2046.

Audétat, A., and Simon, A.C., 2012, Magmatic controls on porphyry Cu genesis: Society of Economic Geologists, Special Publication 16, p. 553–572.

Audétat, A., Pettke, T., and Dolejš, D., 2004, Magmatic anhydrite and calcite in the ore-forming quartz-monzodiorite magma at Santa Rita, New Mexico (USA): Genetic constraints on porphyry-Cu mineralization: Lithos, v. 72, p. 147–161.

Baker, D.R., and Moretti, R., 2011, Modeling the solubility of sulfur in magmas: A 50-year old geochemical challenge: Reviews in Mineralogy and Geochemistry, v. 73, p. 167–213.

Bell, A.S., Simon, A., and Guillong, M., 2009, Experimental constraints on Pt, Pd and Au partitioning and fractionation in silicate melt-sulfide-oxide-aqueous fluid systems at 800°C, 150MPa and variable sulfur fugacity: Geochimica et Cosmochimica Acta, v. 73, p. 5778–5792.

Biek, R.F., 2006, Geology of the Rose Canyon area, Salt Lake County, Utah—the exhumed flank of the Bingham volcanic center: Utah Geological Survey, Open-File Report 475, p. 24–49.

Biek, R.F., Keith, J.D., Solomon, B.J., and Smith, T.W., 2005, Geologic map of the Tickville Spring Quadrangle, Salt Lake and Utah counties, Utah: Utah Geological Survey, Map 214, scale 1:24,000, 2 plates.

Biek, R.F., Solomon, B.J., Smith, T.W., and Keith, J.D., 2007, Geologic map of the Copperton Quadrangle, Salt Lake county, Utah: Utah Geological Survey, Map 219, scale 1:24,000, 1 plate.

Brenan, J.M., 2015, Se-Te fractionation by sulfide-silicate melt partitioning: Implications for the composition of mantle-derived magmas and their melting residues: Earth and Planetary Science Letters, v. 422, p. 45–57.

Candela, P.A., and Holland, H.D., 1984, The partitioning of copper and molybdenum between melts and aqueous fluids: Geochimica et Cosmochimica Acta, v. 48, p. 373–380.

Cassidy, M., Edmonds, M., Watts, S.F., Palmer, M.R., and Gernon, T.M., 2015, Origin of basalt by hybridization in andesite-dominated arcs: Journal of Petrology, v. 56, p. 325–346.

Chambefort, I., Dilles, J.H., and Kent, A.J., 2008, Anhydrite-bearing andesite and dacite as a source for sulfur in magmatic-hydrothermal mineral deposits: Geology, v. 36, p. 719–722.

Chesley, J.T., and Ruiz, J., 1997, Preliminary Re-Os dating on molybdenite mineralization from the Bingham Canyon porphyry copper deposit, Utah: Society of Economic Geologists, Guidebook Series, v. 29, p. 165–169.

Chiaradia, M., Merino, D., and Spikings, R., 2009, Rapid transition to long-lived deep crustal magmatic maturation and the formation of giant porphyry-related mineralization (Yanacocha, Peru): Earth and Planetary Science Letters, v. 288, p. 505–515.

Cloos, M., 2001, Bubbling magma chambers, cupolas, and porphyry copper deposits: International Geology Review, v. 43, p. 285–311.

Collins, S.J., Pyle, D.M., and Maclennan, J., 2009, Melt inclusions track pre-eruption storage and dehydration of magma at Etna: Geology, v. 37, p. 571–574.

Coogan, L.A., Saunders, A.D., and Wilson, R.N., 2014, Aluminum-in-olivine thermometry of primitive basalts: Evidence of an anomalously hot mantle source for large igneous provinces: Chemical Geology, v. 368, p. 1–10.

Core, D.P., Kesler, S.E., and Essene, E.J., 2006, Unusually Cu-rich magmas associated with giant porphyry copper deposits: Evidence from Bingham, Utah: Geology, v. 34, p. 41–44.

Danyushevsky, L.V., Della-Pasqua, F.N., and Sokolov, S., 2000, Re-equilibration of melt inclusions trapped by magnesian olivine phenocrysts from subduction-related magmas: Petrological implications: Contributions to Mineralogy and Petrology, v. 138, p. 68–83.

Deino, A., and Keith, J.D., 1997, Distribution of gold and silver in the Bingham Canyon porphyry copper deposit: Society of Economic Geologists, Guidebook Series, v. 29, p. 91–100.
Dilles, J.H., 1987, Petrology of the Yerington batholith, Nevada: Evidence for evolution of porphyry copper ore fluids: Economic Geology, v. 82, p. 1750–1789.
Ducea, M.N., and Barton, M.D., 2007, Igniting flare-up events in Cordilleran arcs: Geology, v. 35, p. 1047–1050.
Ducea, M.N., Paterson, S.R., and Decelles, P.G., 2015, High-volume magmatic events in subduction system: Elements, v. 11, p. 99–104.
Eichelberger, J.C., 1978, Andesitic volcanism and crustal evolution: Nature, v. 275, p. 21–27.
Elburg, M., Kamenetsky, V.S., Nikogosian, I., Foden, J., and Sobolev, A.V., 2006, Coexisting high- and low-calcium melts identified by mineral and melt inclusion studies of a subduction-influenced syn-collisional magma from South Sulawesi, Indonesia: Journal of Petrology, v. 47, p. 2433–2462.
Elkins-Tanton, L.T., Draper, D.S., Agee, C.B., Jewell, J., Thorpe, A., and Hess, P.C., 2007, The last lavas erupted during the main phase of the Siberian flood volcanic province: Results from experimental petrology: Contributions to Mineralogy and Petrology, v. 153, p. 191–209.
English, J.M., and Johnston, S.T., 2004, The Laramide orogeny: What were the driving forces?: International Geology Review, v. 46, p. 833–838.
Guillong, M., and Heinrich, C.A., 2007, Sensitivity enhancement in laser ablation ICP-MS using small amounts of hydrogen in the carrier gas: Journal of Analytical Atomic Spectrometry, v. 22, p. 1488–1494.
Halter, W.E., Pettke, T., and Heinrich, C.A., 2004a, Laser-ablation ICP-MS analysis of silicate and sulfide melt inclusions in an andesitic complex I: Analytical approach and data evaluation: Contributions to Mineralogy and Petrology, v. 147, p. 385–396.
Halter, W.E., Heinrich, C.A., and Pettke, T., 2004b, Laser-ablation ICP-MS analysis of silicate and sulfide melt inclusions in an andesitic complex II: Evidence for magma mixing and magma chamber evolution: Contributions to Mineralogy and Petrology, v. 147, p. 397–412.
Halter, W.E., Heinrich, C.A., and Pettke, T., 2005, Magma evolution and the formation of porphyry Cu-Au ore fluids: Evidence from silicate and sulfide melt inclusions: Mineralium Deposita, v. 39, p. 845–863.
Hattori, K., 1993, High-sulfur magma, a product of fluid discharge from underlying mafic magma: Evidence from Mount Pinatubo, Philippines: Geology, v. 21, p. 1083–1086.
Hattori, K.H., and Keith, J.D., 2001, Contribution of mafic melt to porphyry copper mineralization: Evidence from Mount Pinatubo, Philippines, and Bingham Canyon, Utah, USA: Mineralium Deposita, v. 36, p. 799–806.
Heinrich, C.A., Driesner, T., Stefánsson, A., and Seward, T.M., 2004, Magmatic vapor contraction and the transport of gold from the porphyry environment to epithermal ore deposits: Geology, v. 32, p. 761–764.
Hernon, R.M., Jones, W.R., and Moore, S.L., 1964, Geology of the Santa Rita Quadrangle, New Mexico: U.S. Geological Survey, Quadrangle Map GQ-306, scale 1:24,000, 1 sheet.
Holland, T., and Blundy, J., 1994, Non-ideal interactions in calcic amphiboles and their bearing on amphibole-plagioclase thermometry: Contributions to Mineralogy and Petrology, v. 116, p. 433–447.
Hou, Z.Q., Yang, Z.M., Lu, Y., Kemp, A., Zheng, Y., Li, Q., Tang, J.X., Yang, Z.S., and Duan, L., 2015, A genetic linkage between subduction- and collision-related porphyry Cu deposits in continental collision zones: Geology, v. 43, p. 247–250.
Hunt, J.P., 1991, Porphyry copper deposits: Economic Geology Monograph, v. 8, p. 192–206.
Irving, A.J., and Green, D.H., 2008, Phase relationships of hydrous alkalic magmas at high pressures: Production of nepheline hawaiitic to mugearitic liquids by amphibole-dominated fractional crystallization within the lithospheric mantle: Journal of Petrology, v. 49, p. 741–756.
Janssen, A., Putnis, A., and Geisler, T., 2010, The experimental replacement of ilmenite by rutile in HCl solutions: Mineralogical Magazine, v. 74, p. 633–644.
Jenner, F.E., O'Neill, H.S.C., Arculus, R.J., and Mavrogenes, J.A., 2010, The magnetite crisis in the evolution of arc-related magmas and the initial concentration of Au, Ag and Cu: Journal of Petrology, v. 51, p. 2445–2464.
Jochum, K.P., Weis, U., Stoll, B., Kuzmin, D., Yang, Q., Raczek, I., Jacob, D.E., Stracke, A., Birbaum, K., Frick, D.A., Günther, D., and Enzweiler, J., 2011, Determination of reference values for NIST SRM 610-617 glasses following ISO guidelines: Geostandards and Geoanalytical Research, v. 35, p. 397–429.
Johnson, E.R., Kamenetsky, V.S., and McPhie, J., 2013, The behavior of metals (Pb, Zn, As, Mo, Cu) during crystallization and degassing of rhyolites from the Okataina volcanic center, Taupo volcanic zone, New Zealand: Journal of Petrology, v. 54, p. 1641–1659.
Jones, W.R., Hernon, R.M., and Moore, S.L., 1967, General geology of the Santa Rita quadrangle, Grant Country, New Mexico: U.S. Geological Survey, Professional Paper 555, 144 p.
Jugo, P.J., Wilke, M., and Botcharnikov, R.E., 2010, Sulfur K-edge XANES analysis of natural and synthetic basaltic glasses: Implications for S speciation and S content as function of oxygen fugacity: Geochimica et Cosmochimica Acta, v. 74, p. 5926–5938.
Karlstrom, K.E., Whitmeyer, S.J., Dueker, K., Williams, M.L., Levander, A., Humphreys, G., Keller, G.R., and CD-ROM Working Group, 2005, Synthesis of results from the CD-ROM experiment: 4-D image of the lithosphere beneath the Rocky Mountains and implications for understanding the evolution of continental lithosphere: Geophysical Monograph, v. 154, p. 421–441.
Keith, J.D., Whitney, J.A., Hattori, K., Ballantyne, G.H., Christiansen, E.H., Barr, D.L., Cannan, T.M., and Hook, C.J., 1997, The role of magmatic sulfides and mafic alkaline magmas in the Bingham and Tintic mining district, Utah: Journal of Petrology, v. 38, p. 1679–1690.
Kelley, K.A., Plank, T., Newman, S., Stolper, E.M., Grove, T.L., Parman, S., and Hauri, E.H., 2010, Mantle melting as a function of water content beneath the Mariana arc: Journal of Petrology, v. 51, p. 1711–1738.
Kent, A.J.R., 2008, Melt inclusions in basaltic and related volcanic rocks: Reviews in Mineralogy and Geochemistry, v. 69, p. 273–331.
Kent, A.J.R., Darr, C., Koleszar, A.M., Salisbury, M.J., and Cooper, K.M., 2010, Preferential eruption of andesitic magmas through recharge filtering: Nature Geoscience, v. 3, p. 631–636.
Keppler, H., and Wyllie, P.J., 1991, Partitioning of Cu, Sn, Mo, W, U, and Th between melt and aqueous fluid in the system haplogranite-H_2O-HCl and haplogranite-H_2O-HF: Contributions to Mineralogy and Petrology, v. 109, p. 139–150.
Kullerud, G., Yund, R.A., and Moh, G.H., 1969, Phase relations in the CuFe-S, Cu-Ni-S and Fe-Ni-S systems: Economic Geology Monograph 4, p. 323–343.
Landtwing, M.R., Furrer, C., Redmond, P.B., Pettke, T., Guillong, M., and Henry, C.A., 2010, The Bingham Canyon porphyry Cu-Mo-Au deposit. III. Zoned copper-gold ore deposition by magmatic vapor expansion: Economic Geology, v. 105, p. 91–118.
Larocque, A.C., Stimac, Y.E.S., Keith, J.D., and Huminicki, M.A., 2000, Evidence for open-system behavior in immiscible Fe-S-O liquids in silicate magmas: Implications for contributions of metals and sulfur to ore-forming fluids: Canadian Mineralogist, v. 38, p. 1233–1249.
Lepage, L.D., 2003, ILMAT: An Excel worksheet for ilmenite-magnetite geothermometry and geobarometry: Computers and Geosciences, v. 29, p. 673–678.
Leslie, R.A., Danyushevsky, L.V., Crawford, A.J., and Verbeeten, A.C., 2009, Primitive shoshonites from Fiji: Geochemistry and source components: Geochemistry, Geophysics, Geosystems, v. 10, 24 p., doi: 10.1029/2008GC002326.
Li, Y., and Audétat, A., 2012, Partitioning of V, Mn, Co, Ni, Cu, Zn, As, Mo, Ag, Sn, Sb, W, Au, Pb, and Bi between sulfide phases and hydrous basanite melt at upper mantle conditions: Earth and Planetary Science Letters, v. 355–356, p. 327–340.
——2015, Effects of temperature, silicate melt composition, and oxygen fugacity on the partitioning of V, Mn, Co, Ni, Cu, Zn, As, Mo, Ag, Sn, Sb, W, Au, Pb, and Bi between sulfide phases and silicate melt: Geochimica et Cosmochimica Acta, v. 162, p. 25–45.
Liu, X., Xiong, X., Audétat, A., Li, Y., Song, M.H., Li, L., Sun, W.D., and Ding, X., 2014, Partitioning of copper between olivine, orthopyroxene, clinopyroxene, spinel, garnet and silicate melts at upper mantle conditions: Geochimica et Cosmochimica Acta, v. 125, p. 1–22.
Liu, X., Xiong, X., Audétat, A., and Li, Y., 2015, Partitioning of Cu between mafic minerals, Fe-Ti oxides and intermediate to felsic melts: Geochimica et Cosmochimica Acta, v. 151, p. 86–102.
Lloyd, A.S., Plank, T., Ruprecht, P., Hauri, E.H., and Rose, W., 2013, Volatile loss from melt inclusions in pyroclasts of differing sizes: Contributions to Mineralogy and Petrology, v. 165, p. 129–153.
Loucks, R.R., 2014, Distinctive composition of copper-ore-forming arc magmas: Australian Journal of Earth Sciences, v. 61, p. 5–16.
Luhr, J.F., 2008, Primary igneous anhydrite: Progress since its recognition in the 1982 El Chichón trachyandesite: Journal of Volcanology and Geothermal Research, v. 175, p. 394–407.

Maria, A.H., and Luhr, J.F., 2008, Lamprophyres, basanites, and basalts of the western Mexican volcanic belt: Volatile contents and a vein-wallrock melting relationship: Journal of Petrology, v. 49, p. 2123–2156.
Masotta, M., and Keppler, H., 2015, Anhydrite solubility in differentiated arc magmas: Geochimica et Cosmochimica Acta, v. 158, p. 79–102.
Maughan, D.T., Keith, J.D., Christiansen, E.H., Pulsipher, T., Hattori, K., and Evans, N.J., 2002, Contributions from mafic alkaline magmas to the Bingham porphyry Cu-Au-Mo deposit, Utah, USA: Mineralium Deposita, v. 37, p. 14–37.
McLemore, V.T., 2008, Potential for Laramide porphyry copper deposits in southwestern New Mexico: New Mexico Geological Society, 59th Annual Field Conference Guidebook, p. 141–149.
McMillan, W.J., 2005, Porphyry Cu-Mo deposits of the Highland Valley district, Guichon Creek batholith, British Columbia, Canada, *in* Porter T.M., ed., Super porphyry copper and gold deposits—a global perspective, v. 1: Adelaide, PGC Publishing, p. 259–274.
Métrich, N., and Deloule, E., 2014, Water content, δD and δ^{11}B tracking in the Vanuatu arc magmas (Aoba Island): Insights from olivine-hosted melt inclusions: Lithos, v. 206, p. 400–408.
Mizer, J.D., Barton, M.D., and Stegen, R.J., 2015, U-Pb geochronology of Laramide magmatism related to Cu-, Zn-, and Fe-mineralized systems, Central mining district, New Mexico, *in* Pennell, W.M., and Garside, L.J., eds., Geological Society of Nevada 2015 Symposium: New Concepts and Discoveries, v. 2: Lancaster, DEStech Publication, Inc., p. 1109–1129.
Moore, W.J., 1973, Igneous rocks in Bingham mining district, Utah: U.S. Geological Survey, Professional Paper 629-B, 41 p.
Mpodozis, C., and Cornejo, P., 2012, Cenozoic tectonics and porphyry copper systems of the Chilean Andes: Society of Economic Geologists, Special Publication 16, p. 329–360.
Mutschler, F.E., Ludington, S., and Bookstrom, A.A., 1999, Giant porphyry-related metal camps of the world—a database: U.S. Geological Survey, Open-File Report 99-556, http://pubs.usgs.gov/of/1999/of99-556/.
Nadeau, O., Williams-Jones, A.E., and Stix, J., 2010, Sulphide magma as a source of metals in arc-related magmatic hydrothermal ore fluids: Nature Geoscience, v. 3, p. 501–505.
Pallister, J.S., Hoblitt, R.P., Meeker, G.P., Knight, R.J., and Siems, D.F., 1996, Magma mixing at Mount Pinatubo: Petrographic and chemical evidence from the 1991 deposits, *in* Newhall, C., and Punongbayan, R., eds., Fire and mud: Eruptions and lahars of Mount Pinatubo, Philippines: Seattle, London, University of Washington Press, p. 687–731.
Parat, F., Holtz, F., and Streck, M.J., 2011, Sulfur-bearing magmatic accessory minerals: Reviews in Mineralogy and Geochemistry, v. 73, p. 285–314.
Parry, W.T., Wilson, P.N., Moser, D., and Heizler, M.T., 2001, U-Pb dating of zircon and ^{40}Ar/^{39}Ar dating of biotite at Bingham, Utah: Economic Geology, v. 96, p. 1671–1683.
Pettke, T., 2006, In situ laser-ablation-ICP-MS chemical analysis of melt inclusions and prospects for constraining subduction zone magmatism: Mineralogical Association of Canada, Short Course Series, v. 36, p. 51–80.
Pettke, T., Oberli, F., and Heinrich, C.A., 2010, The magma and metal source of giant porphyry-type ore deposits, based on lead isotope microanalysis of individual fluid inclusions: Earth and Planetary Science Letters, v. 296, p. 267–277.
Plank, T., Kelley, K.A., Zimmer, M.M., Hauri, E.H., and Wallace, P.J., 2013, Why do mafic arc magmas contain ~4 wt % water on average?: Earth and Planetary Science Letters, v. 364, p. 168–179.
Pollard, P.J., Taylor, R.G., and Peters, L., 2005, Ages of intrusion, alteration, and mineralization at the Grasberg Cu-Au deposit, Papua, Indonesia: Economic Geology, v. 100, p. 1005–1020.
Portnyagin, M., Hoernle, K., Plechov, P., Mironov, N., and Khubunaya, S., 2007, Constraints on mantle melting and composition and nature of slab components in volcanic arcs from volatiles (H_2O, S, Cl, F) and trace elements in melt inclusions from the Kamchatka arc: Earth and Planetary Science Letters, v. 255, p. 53–69.
Reubi, O., and Blundy, J., 2009, A dearth of intermediate melts at subduction zone volcanoes and the petrogenesis of arc andesites: Nature, v. 461, p. 1269–1273.
Richards, J.P., 2003, Tectono-magmatic precursors for porphyry Cu-(Mo-Au) deposit formation: Economic Geology, v. 98, p. 1515–1533.
——2005, Cumulative factors in the generation of giant calc-alkaline porphyry Cu deposits, *in* Porter, T.M., ed., Super porphyry copper and gold deposits, v. 1: A global perspective: Adelaide, PGC Publishing, p. 7–25.
——2009, Postsubduction porphyry Cu-Au and epithermal Au deposits: Products of remelting of subduction-modified lithosphere: Geology, v. 37, p. 247–250.
——2011, High Sr/Y arc magma and porphyry Cu ± Mo ± Au deposits: Just add water: Economic Geology, v. 106, p. 1075–1081.
Righter, K., and Carmichael, I.S., 1996, Phase equilibria of phlogopite lamprophyres from western Mexico: Biotite-liquid equilibria and PT estimates for biotite-bearing igneous rocks: Contributions to Mineralogy and Petrology, v. 123, p. 1–21.
Rodríguez, C., Sellés, D., Dungan, M., Langmuir, C., and Leeman, W., 2007, Adakitic dacites formed by intracrustal crystal fractionation of water-rich magma parent at Nevado de Longavi volcano (36.2°S; Andean Southern volcanic zone, central Chile): Journal of Petrology, v. 48, p. 2033–2061.
Saito, G., Morishita, Y., and Shinohara, H., 2010, Magma plumbing system of the 2000 eruption of Miyakejima volcano, Japan, deduced from volatile and major component contents of olivine-hosted melt inclusions: Journal of Geophysical Research-Solid Earth, v. 115, 29 p., doi: 10.1029/2010JB007433.
Seo, J.H., Guillong, M., and Heinrich, C.A., 2012, Separation of molybdenum and copper in porphyry deposits: The roles of sulfur, redox, and pH in ore mineral deposition at Bingham Canyon: Economic Geology, v. 107, p. 335–356.
Sillitoe, R.H., 2010, Porphyry copper systems: Economic Geology, v. 105, p. 3–41.
Słaby, E., and Martin, H., 2008, Mafic and felsic magma interaction in granites: The Hercynian Karkonosze pluton (Sudetes, Bohemian Massif): Journal of Petrology, v. 49, p. 353–391.
Smith, D.R., and Leeman, W.P., 1987, Petrogenesis of Mount St. Helens dacitic magma: Journal of Geophysical Research-Solid Earth, v. 92, p. 10,313–10,334.
——1993, The origin of Mount St. Helens andesites: Journal of Volcanology and Geothermal Research, v. 55, p. 271–303.
Stavast, W.J.A., Keith, J.D., Christiansen, E.H., Dorais, M.J., Tingey, D., Larocque, A., and Evans, N., 2006, The fate of magmatic sulfides during intrusion or eruption, Bingham and Tintic districts, Utah: Economic Geology, v. 101, p. 329–345.
Steinberger, I., Hinks, D., Driesner, T., and Heinrich, C.A., 2013, Source plutons driving porphyry copper ore formation: Combining geomagnetic data, thermal constraints, and chemical mass balance to quantify the magma chamber beneath the Bingham Canyon deposit: Economic Geology, v. 108, p. 605–624.
Stern, C.R., Funk, J.A., Skewes, M.A., and Arévalo, A., 2007, Magmatic anhydrite in plutonic rocks at the El Teniente Cu-Mo deposit, Chile, and the role of sulfur-and copper-rich magmas in its formation: Economic Geology, v. 102, p. 1335–1344.
Stewart, J.H., Moore, W.J., and Zietz, I., 1977, East-west patterns of Cenozoic igneous rocks, aeromagnetic anomalies, and mineral deposits, Nevada and Utah: Geological Society of America Bulletin, v. 88, p. 67–77.
Stormer, J.C., 1983, The effects of recalculation on estimates of temperature and oxygen fugacity from analyses of multi-component iron-titanium oxides: American Mineralogist, v. 68, p. 586–594.
Sun, W.D., Bennett, V.C., and Kamenetsky, V.S., 2004a, The mechanism of Re enrichment in arc magmas: Evidence from Lau Basin basaltic glasses and primitive melt inclusions: Earth and Planetary Science Letters, v. 222, p. 101–114.
Sun, W.D., Arculus, R.J., Kamenetsky, V.S., and Binns, R.A., 2004b, Release of gold-bearing fluids in convergent margin magmas prompted by magnetite crystallization: Nature, v. 431, p. 975–978.
Vaggelli, G., Pellegrini, M., Vougioukalakis, G., Innocenti, S., and Francalanci, L., 2009, Highly Sr radiogenic tholeiitic magmas in the latest inter-Plinian activity of Santorini volcano, Greece: Journal of Geophysical Research-Solid Earth, v. 114, 21 p., doi: 10.1029/2008JB005936.
van Dongen, M., Vineyard, R.F., Tomkins, A.G., Armstrong, R.A., and Woodhead, J.D., 2010, Recycling of Proterozoic crust in Pleistocene juvenile magma and rapid formation of the Ok Tedi porphyry Cu-Au deposit, New Guinea: Lithos, v. 114, p. 282–292.
Vigouroux, N., Wallace, P.J., and Kent, A.J., 2008, Volatiles in high-K magmas from the western Trans-Mexican volcanic belt: Evidence for fluid fluxing and extreme enrichment of the mantle wedge by subduction processes: Journal of Petrology, v. 49, p. 1589–1618.
von Quadt, A., Erni, M., Martinek, K., Moll, M., Peytcheva, I., and Heinrich, C.A., 2011, Zircon crystallization and the lifetimes of ore-forming magmatic-hydrothermal systems: Geology, v. 39, p. 731–734.
Waite, K.A., Keith, J.D., Christiansen, E.H., Whitney, J.A., Hattori, K., Tingey, D.T., and Hook, C.J., 1997, Petrogenesis of the volcanic and intrusive rocks associated with the Bingham porphyry Cu-Mo deposit, Utah: Society of Economic Geologists, Guidebook Series, v. 29, p. 69–90.

Wallace, P.J., and Edmonds, M., 2011, The sulfur budget in magmas: Evidence from melt inclusions, submarine glasses, and volcanic gas emissions: Reviews in Mineralogy and Geochemistry, v. 73, p. 215–246.

Watson, E.B., and Harrison, T.M., 1983, Zircon saturation revisited: Temperature and composition effects in a variety of crustal magma types: Earth and Planetary Science Letters, v. 64, p. 295–304.

Webster, J.D., 2004, The exsolution of magmatic hydrosaline chloride liquids: Chemical Geology, v. 210, p. 33–48.

Webster, J.D., Vetere, F., Botcharnikov, R.E., Goldoff, B., McBirney, A., and Doherty, A.L., 2015, Experimental and modeled chlorine solubilities in aluminosilicate melts at 1 to 7000 bars and 700 to 1250°C: Applications to magmas of Augustine volcano, Alaska: American Mineralogist, v. 100, p. 522–535.

Witter, J.B., Kress, V.C., and Newhall, C.G., 2005, Volcán Popocatépetl, Mexico. Petrology, magma mixing, and immediate sources of volatiles for the 1994–present eruption: Journal of Petrology, v. 46, p. 2337–2366.

Xiao, B., Qin, K., Li, G., Li, J., Xia, D., Chen, L., and Zhao, J., 2012, Highly oxidized magma and fluid evolution of Miocene Qulong giant porphyry Cu-Mo deposit, southern Tibet, China: Resource Geology, v. 62, p. 4–18.

Zajacz, Z., and Halter, W., 2007, LA-ICPMS analyses of silicate melt inclusions in co-precipitated minerals: Quantification, data analysis and mineral/melt partitioning: Geochimica et Cosmochimica Acta, v. 71, p. 1021–1040.

——2009, Copper transportation by high temperature, sulfur-rich magmatic vapor: Evidence from silicate melt inclusions and vapor in a basaltic andesite from the Villarrica volcano (Chile): Earth and Planetary Science Letters, v. 282, p. 115–121.

Zajacz, Z., Seo, J.H., Candela, P.A., Piccoli, P.M., Heinrich, C.A., and Guillong, M., 2010, Alkali metals control the release of gold from volatile-rich magmas: Earth and Planetary Science Letters, v. 297, p. 50–56.

Zhang, L., and Audétat, A., 2016, Diffusional modification of Cu concentrations in melt inclusions: ETH Zürich, Fifteenth International Symposium on Experimental Mineralogy, Petrology and Geochemistry, Zurich, Switzerland, June 5–8, 2016, Abstract P11.